TAMPEREEN TEKNILLINEN YLIOPISTO
TAMPERE UNIVERSITY OF TECHNOLOGY

Leena Jaatinen

The Effect of an Applied Electric Current on Cell Proliferation, Viability, Morphology, Adhesion, and Stem Cell Differentiation

Julkaisu 1462 • Publication 1462

Tampere 2017

Tampereen teknillinen yliopisto. Julkaisu 1462
Tampere University of Technology. Publication 1462

Leena Jaatinen

The Effect of an Applied Electric Current on Cell Proliferation, Viability, Morphology, Adhesion, and Stem Cell Differentiation

Thesis for the degree of Doctor of Science in Technology to be presented with due permission for public examination and criticism in Tietotalo Building, Auditorium TB109, at Tampere University of Technology, on the 7th of April 2017 at 12 noon.

Tampereen teknillinen yliopisto - Tampere University of Technology
Tampere 2017

ISBN 978-952-15-3918-3 (printed)
ISBN 978-952-15-3940-4 (PDF)
ISSN 1459-2045

Abstract

The importance of electrical stimulus is often underrated in cell biology and tissue engineering, although electric fields and currents, both endogenous and applied, play a great role in many cellular functions. Electrical stimulation of the cells causes direct effects on cells, such as rearrangement of the cytoskeleton, redistribution of membrane receptors and changes in calcium dynamics, as well as electrochemical reactions at the electrode/electrolyte interface. In this thesis, the effect of an applied electric current on cell proliferation, viability, morphology, adhesion, and stem cell differentiation was studied. The electric stimulation was applied to two different types of mammalian cells, mouse myoblasts and adipose-derived stem cells that were either in a direct contact with the electrodes or in a contact with the electrodes through the electrolyte.

The applied electric current changed the cell spreading characteristics on the electrode, and induced the more elongated cell morphology even when the cells were not cultured directly on the electrode. However, after a certain threshold, the increase in current dose resulted in decrease in the cell viability and sometimes also on the cell proliferation rates. The stimulation influenced the cell adhesion as well, studied by both quantitative and qualitative methods on the electrode and in a biomaterial scaffold. The low currents decreased and higher currents increased the cell-substrate adhesion forces. The highest adhesion forces were related to the poor cell viability and at the highest current values, it was impossible to detach the cell from the substrate. The increase in electric current also decreased the cell migration and adhesion to the scaffold. In addition to the changes in their morphology, the stimulation of the adipose-derived stem cells also modified their differentiation pattern. Stimulation of the stem cells with electric current and electrochemically released Cu^{2+} induced the up-regulation of neuron-specific genes and proteins, whereas stimulation with current only mainly induced changes in the cell morphology.

As demonstrated in this thesis, electric stimulation induces changes in many cellular functions and might offer an easy and cost-effective method to regulate them in future *in vitro* and *in vivo* applications. For instance, electric current could be used for

controlled arrangement of cells within the scaffold or for inducing the neuronal differentiation of stem cells.

Acknowledgements

The very first part of this thesis started in Finland, and I would like to express my gratitude to all the people who contributed during that time, especially Katja Ahtiainen, Susanna Miettinen, Minna Kellomäki, Soile Lönnqvist, Baran Aydogan, and my supervisor prof. Jari Hyttinen, whom I would like to thank for all the support and for giving me the opportunity to go to the ETH Zürich. Prof. Janos Vörös, thank you so much for warmly welcoming me to your group, giving me all the support I could have possibly asked for and never making me feel like an outsider. Tomaso Zambelli, thank you for being my unofficial FluidFM supervisor, and Esther Singer, Martin Lanz and Stephen Wheeler for making my stay at the LBB as smooth and nice as possible, and especially Stephen for all the amazing bits and parts I needed for my experiments, and the nice chats about football. Daniel Eberli, Souzan Salemi, and Sarah Nötzli, I am so happy I got to collaborate with your group at the Unispital Zürich, this thesis would have never been finished without you. I am grateful for the financial support of the Finnish Cultural Foundation, and Janos Vörös and Daniel Eberli for covering the material costs throughout this thesis.

I would also like to thank my students, Davide Boffa, Ramon Mägert, and Eleanore Young for all being such good students and truly helping me with this thesis. Pablo Dörig for introducing me to the FluidFM, doing the first experiments with me, and always being there for me. Laszlo Demko, I am forever grateful for your contribution to my last paper, and also for not complaining too much when we are together at the gym.

The whole amazing LBB group who made my time at the LBB unforgettable. Norma and Elsa, you are very important to me and I enjoy everything we did and will do together. Rami, just for being there and always supporting me. Peter, for being my mountain buddy and still keeping up my hopes you will come back one day. Victoria

and Raphael, thank you for all the parties, dinners, lunches and even hikes we did together. Prayanka, thank you for being such an amazing office mate, for inviting me to your wedding, teaching me how to cook Indian curry and teasing Alex T with me. Alex T. for being the most amazing Johnny Bravo. Harald, Juliane, Orane, Bernd, Benji, Klas, Alex L, Dariiiio, Gemma, Raphael G, Chris, Queralt, Tatiana, Kaori, Sophie, Florian, all of you who have already left but who I will never forget. Mathias, Luca, Serge, Raphael T, Andreas, Vincent, Flurin, Stephanie, Livie, Hana, Greta, all of you who are still there one way or another and who keep inviting me to the parties and are always happy to have a coffee and a chat with me.

Last but not least I want to thank my family; Lucas, äiti, isä, Tuomas and Laine, Matti, Outi and Aatu, Taina, Saku and Tuuli, and Tiina, as well as all my friends in Finland, Switzerland and all over the world. You did not necessarily contribute directly to my thesis but you kept me sane and on the good mood during the whole process.

Contents

List of original publications

I. **Jaatinen L**., Mäenpää K., Sippola L., Suuronen R., Kellomäki M., Ylikomi T., Miettinen S. and Hyttinen J. Bioimpedance measurement setup for the assessment of viability and number of human adipose stem cells cultured as monolayers. IFMBE Proceedings 2009 25/10 pp. 286-88

II. **Jaatinen L**., Salemi S., Miettinen S., Hyttinen J., Eberli D. The combination of electric current and copper promotes neuronal differentiation of adipose-derived stem cells. Annals of Biomedical Engineering 2015 43 (4) pp. 1014-23

III. **Jaatinen L**., Vörös J., Hyttinen J., Controlling cell migration and adhesion into a scaffold by external electric currents. Conference proceedings IEEE Engineering in Medicine and Biology Society 2015 pp. 3549-52

IV. **Jaatinen L**., Young E., Hyttinen J., Vörös J., Zambelli T., Demkó L. Quantifying the effect of electric current on cell adhesion studied by single-cell force spectroscopy. Biointerphases 2016 11 (1) p. 011004

Author`s contributions

I. The author designed and performed the impedance measurement experiments in collaboration with the second author. The author analyzed the data and wrote the manuscript as the first author.

II. The author designed and performed the experiments as well as analyzed the data and wrote the manuscript in an equal contribution with the second author.

III. The author designed and performed the experiments, analyzed the data and wrote the manuscript as the first author.

IV. The author designed the experiments and performed the force spectroscopy measurements in collaboration with the last author and the immunohistochemical experiments in collaboration with the second author. The author analyzed the data and wrote the manuscript in collaboration with the last author.

Abbreviations

2D	Two-dimensional
3D	Three-dimensional
AC	Alternating current
ADSC	Adipose-derived stem cells
AFM	Atomic force microscopy
ATP	Adenosine triphosphate
BHA	Butylated hydroxyanisole
BME	β-mercaptoethanol
BSA	Bovine serum albumin
C2C12	Mouse myoblast
CV	Cyclic voltammetry
DAPI	4',6-diamidino-2-phenylindole
DC	Direct current
DMEM	Dulbecco`s modified Eagle medium
DMSO	Dimethylsulfoxide
DNA	Deoxyribonucleic acid
EF	Electric field
FACS	Fluorescence-activated cell sorter
FAK	Focal adhesion kinase
FBS	Fetal bovine serum

FluidFM	Fluidic force microscopy
HEK	Human Embryonic Kidney cell
HeLa	Human cervical cancer cell
HUVEC	Human Umbilical Vascular E dothelial Cell
hMSC	Human mesenchymal stem cell
IPSC	Induced pluripotent stem cell
ITO	Indium tin oxide
MAP	Mitogen kinase protein
MAP-2	Microtubule-associated protein 2
mRNA	Messenger ribonucleic acid
PBS	Phosphate buffered saline
PCR	Polymerase chain reaction
PDMS	Polydimethylsiloxane
PLA	Polylactide
PLC	Phospholipase C
PEEK	Polyether ether ketone
PS	Phosphatidylserine
ROS	Reactive oxygen species
RT	Room temperature
SCFS	Single-cell force spectroscopy
SDS	Sodium dodecyl sulfate
WB	Western blot

1. Literature review

1.1 Cell migration and adhesion

Cells fall into two categories; adherent and non-adherent cells. Cells that compose tissues and organs are generally adherent cells whereas for instance red blood cells are, and need to be, non-adherent. In the case of adherent cells, adhesion is very essential and vital for the cell survival. Cells either adhere to each other or to the extracellular materials. Adhesion to an extracellular matrix is mediated mainly via proteins called integrins and to other cells via cadherins. Cell-cell junctions are important for instance for anchoring the cells to each other as well as forming channels and relaying signals between the adjacent cells, however, the cell-cell adhesion is not discussed in more detail in this thesis. Figure 1 presents a schematic of a cell adhering to a substrate. Cell adheres to the surface via integrins that bind the actin filaments in the cytoskeleton to the extracellular matrix proteins. In more detail, the intracellular part of the integrin binds to the cytosolic protein talin that in turn binds to the filamentous actin. Also a set of other intracellular linker proteins, such as vinculin are involved in the linkage. Actin filaments are formed by polymerization of globular actin monomers. As the cell adheres, integrins bind and aggregate at the same region, forming focal adhesion points. (Kendall et al. 2011; Alberts et al. 2008)

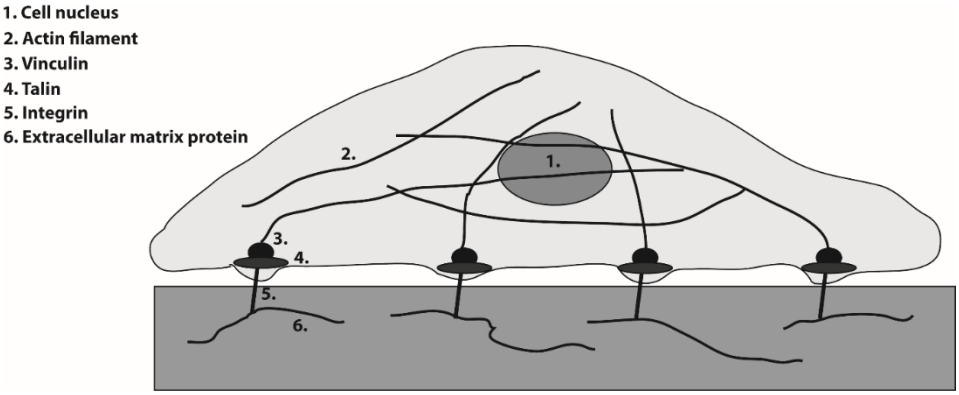

Figure 1. The schematic of a mammalian cell adhered to a substrate. Actin filaments of the cell are connected to the extracellular matrix via integrins and a set of linker proteins such as talin and vinculin. Modified from (Kendall et al. 2011).

There are several factors that affect the cell adhesion, for instance the physical and chemical cues or the substrate characteristics such as elasticity and topography. (Kendall et al. 2011) Cell adhesion is a key factor in many cellular processes, for instance cell migration, tissue repair and regeneration, wound healing, and stem cell differentiation. (Berrier & Yamada 2007)

Cell adhesion is closely related to the cell migration that facilitates proper spatial localization of cells during tissue formation and regeneration. Migration is mainly controlled by chemical and mechanical cues in the microenvironment, such as chemical, mechanical or electric field gradients, and topographical features. (Gumus et al. 2010) In cell migration process, there is a protrusion of flat membrane particles, lamellipodia and filopodia, in the front part of the cell due to the actin polymerization. Next, the adhesion sites in the leading edge, and then in the trailing edge are being assembled and disassembled, and the rear part of the cell lifts off. Myosin-actin interactions control the contractile force than allows the cell migration. (Gunja & Hung 2011)

1.1.1 Measuring cell adhesion

Cell adhesion to a substrate has been traditionally studied with indirect, qualitative methods such as hydrodynamics assays or by analyzing the cell morphology and the size and number of focal adhesion. In hydrodynamic assays, so called washing assays, cells are let to adhere on the substrate and then rinsed with the physiological buffer. The number of the cells that stayed on the substrate is determined by counting. However, the shear forces affecting the cells are unknown and difficult to control. Flow chambers and spinning disc devices offer a better control over the shear forces but these assays still only provide qualitative information about the cell adhesion strength. Another method to qualify cell adhesion is to study the cell morphology such as cell shape, spreading or size that are often related to the adhesion strength. (Taubenberger et al. 2014)

Recently, there has been a great progress in developing quantitative methods for measuring cell adhesion. Quantitative measurement methods are often single-cell force

spectroscopy (SCFS) techniques using micropipettes, magnetic or optical tweezers or atomic force microscopy (AFM). (Taubenberger et al. 2014) AFM is traditionally used for scanning a surface in the x-y plane to obtain topographical images. However, the cantilever can also be scanned in z-direction only for force spectroscopy experiments. Micropipettes and tweezers are usually used to analyze cellular interactions at a single molecule resolution with the forces in piconewton range whereas AFM based SCFS offers a tool to study the adhesion of a whole cell within the detectable force range up to micronewtons. (Guillaume-Gentil et al. 2014)

In a typical AFM-SCFS experiment, the cell is attached to the AFM cantilever prior the adhesion force measurement. This requires the functionalization of the cantilever with a layer of proteins and chemical immobilization of the cell to the cantilever that can be rather cumbersome and time-consuming. The immobilization of the cell can also cause perturbations and thus influence the adhesion force. One of the latest advances is the fluidic force microscopy (FluidFM) that combines the AFM technology with microfluidics within the cantilever. The cell can be immobilized to the cantilever by applying an underpressure through the hollow cantilever that enables the rapid and serial quantification of adhesion forces. (Guillaume-Gentil et al. 2014) FluidFM has already been used in quantifying bacteria (E. coli) (Dörig et al. 2010) and yeast (Potthoff et al. 2012) as well as mammalian cells such as HeLa, HEK (Potthoff et al. 2012) and endothelial cells (Potthoff et al. 2014).

1.2 Stem cell differentiation

Stem cells are non-specialized cells that are capable of both self-renewal and multilineage differentiation. (Weissman 2000) Differentiation is achieved by asymmetric cell division where one daughter cell remains undifferentiated and the other becomes specialized. Stem cells can be either of embryonic (embryonic stem cells) or postnatal (adult stem cells, induced pluripotent stem cells) origin. Embryonic stem cells are pluripotent cells that are able to differentiate to cells from all three embryonic germ layers: endoderm, mesoderm and ectoderm. Induced pluripotent stem cells (IPSCs)

are another type of pluripotent stem cells that are generated from mature adult cells by introducing a set of pluripotency-associated genes. Adult stem cells are found throughout the body and generally able to differentiate into cell types found in the original location of the stem cell although recently it has been shown that they are able to transdifferentiate to other cell types as well and thus show some pluripotency. Adult stem cells are characterized by their origin and the mature cell type they are able to differentiate to. For instance, hematopoietic stem cells are found in the bone marrow and they differentiate to blood cells, and neural stem cells, found in the brain, can give rise to neural cells. Mesenchymal stem cells, derived from for instance placenta, bone marrow or adipose tissue, are capable of differentiating into other mesoderm cells, such as bone and cartilage, but to some extent also for instance to neurons that are found in the ectoderm tissue. In general, many type of stem cells are able to differentiate into neurons (Fig. 2) when exposed to an appropriate stimulus.

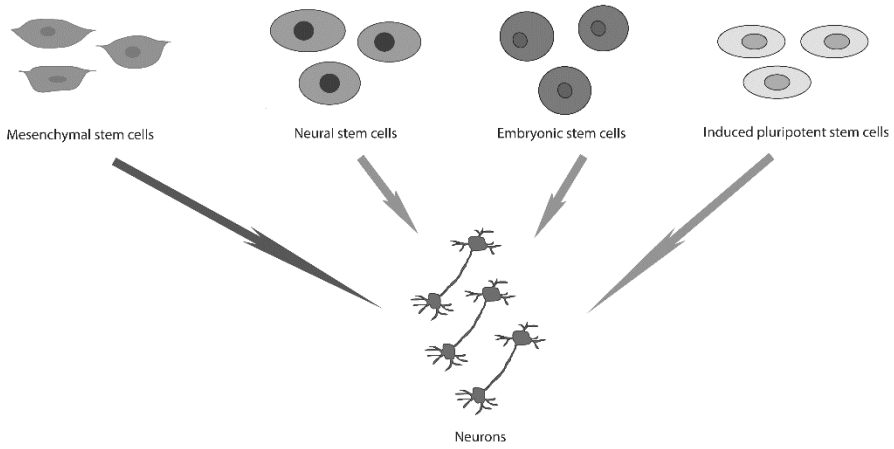

Figure 2. Several different stem cell types, such as mesenchymal stem cells, neural stem cells, embryonic stem cells and induced pluripotent stem cells can differentiate to neurons.

Using adult stem cells as the source for differentiating mature cells causes less ethical issues and decreases the danger of immunogenicity and teratoma formation that are often related to embryonic and induced pluripotent stem cells. (Hentze et al. 2009; Barker & de Beaufort 2013) Compared to other adult stem cells, adipose-derived stem

cells (ADSC) are less scarce and easier to harvest. Studies show that also ADSCs have the capability of neuronal differentiation. (Anghileri et al. 2008; Krampera et al. 2007; Safford et al. 2002) The main methods for differentiating ADSCs to neurons include genetic manipulation, the promotion of neurosphere formation and the use of different cytokines, chemical reagents or growth factors. (Anghileri et al. 2008; Choi et al. 2012; Jang et al. 2010) However, there are issues related to the use the growth factors and chemical reagents; each factor has to be critically reviewed before its use in translational studies, and some reagents currently used for neurogenic differentiation, including dimethylsulfoxide (DMSO), β-mercaptoethanol (BME) and butylated hydroxyanisole (BHA) are criticized due to cell toxicity and induced cell stress. (Lu et al. 2004; Neuhuber et al. 2004)

1.2.1 Neuronal differentiation of stem cells

Due to the limited medical treatment options currently available for neuron repair, there is a clear need for induced regeneration of neural tissues. All the stem cell types, namely embryonic, adult, and induced pluripotent stem cells can give rise to neurons. Of the adult stem cells, for instance bone marrow stromal cells (Sanchez-Ramos et al. 2000), skin (Lebonvallet et al. 2012), dental stem cells (Yang et al. 2014), and adipose-derived stem cells (Safford et al. 2002; Anghileri et al. 2008; Krampera et al. 2007) have been shown to have the capability of neuronal differentiation. The main methods currently used for differentiating adult stem cells toward neurons are genetic manipulation, the promotion of neurosphere formation, and the use of different cytokines, growth factors or chemical reagents. (Choi et al. 2012; Anghileri et al. 2008; Jang et al. 2010) In additional to the traditional methods, the neuronal differentiation triggered by electric stimulation has been studied for instance with neuronal pre-differentiated embryonic stem cells that showed a remarkable increases their differentiation (Yamada et al. 2007) or with embryonic stem cells differentiated to neuronal phenotypes. (Sauer et al. 1999; Ulrich & Majumder 2006) In addition, Matos et al. reported the different effects of alternating electric fields, which were applied through nickel electrodes, on neural stem cell viability and differentiation (Matos & Cicerone 2010). The neuronal differentiation was either enhanced or suppressed

depending on the electric field frequency and the exposure time. Recently it has also been shown that human mesenchymal stem cells (hMSC) have a capability to differentiate into neuron-like cells when cultured on conductive substrate under electric fields (Thrivikraman et al. 2014). Electrical stimulation, along with other physicochemical stimulation, is very cost-effective compared to other methods, for instance using growth factors and other chemical reagents. (Titushkin et al. 2011) There is several mechanisms influencing the differentiation process and it is important to choose carefully the electrical stimulation parameters, such as frequency, intensity and duration. It is possible that stem cells from different origin, for instance embryonic stem cells or adult stem cells, respond differently to an external electrical stimulation because also endogenous electric fields differ in the host tissues. Also the type of voltage-gated ion channels differs between different stem cells types; for instance N-type channels are found only in neuronal tissue which could lead to a completely different response to an applied electric field than in embryonic or mesenchymal stem cells. (Titushkin et al. 2011) Modulating calcium dynamics by electrical stimulus appears to be a powerful method to induce stem cell differentiation. Calcium is able to entry the cell through voltage-gated Ca^{2+} channels. In addition, calcium can be released from intracellular stores, for instance mitochondria. The possible excess calcium is pumped back from cytosol into internal stores or released outside the cells by specific ATPase pumps. Alterations in calcium dynamics can also be an indicator of the level of differentiation; undifferentiated human mesenchymal stem cells (hMSC) have a clearly different calcium oscillation profile than hMSCs that were differentiated to neurogenic or osteogenic phenotypes. (Sun et al. 2007)

In addition to the electric stimulus, another stimulus for triggering and maintaining the neuronal differentiation may be needed. A possible candidate could be copper, as it is found in high concentrations in the central nervous system, and reduced concentrations can be related to several neurological disorders. (Hunt 1980; Weiser & Wienrich 1996) It has been shown that copper is needed for the neurite outgrowth mediated by nerve growth factor signal transduction. (Birkaya & Aletta 2005) Copper also modulates the osteogenic and adipogenic differentiation of mesenchymal stem cells. Presence of copper may be important already at the early stages of stem cell

differentiation as it may take part in both the commitment and maturation steps of the differentiation process. (Rodriguez et al. 2002) Copper, that binds with high affinity to phosphatidylserine (PS), phospholipid enriched especially in neuronal membranes (Monson et al. 2012), may be needed to initiate the ADSC differentiation towards neuronal lineage. In addition, mammalian copper transporter Ctr1 that has been found at plasma membranes and that is responsible of copper transport into the cell, has been suggested to be important in signal transduction mechanism involved in stem cell differentiation. (Haremaki et al. 2007)

1.3 Bioelectricity

Bioelectricity was first discovered in the late 1700s by Luigi Galvani. Bioelectricity means electric potentials and currents produced by or occurring within living cells and tissue. Ionic currents and electric fields play a crucial role in the function of our body. These bioelectric signals are generated by ion channels or pumps, gap junctional connections or epithelial damage. They regulate cellular physiology by inducing changes in transmembrane potential, pH gradients, specific ion flows and electric fields. (Levin 2011) Cells generate a voltage difference of around 70 mV across the plasma membrane, created by the ion gradients that are controlled by the ions pumps moving the ions, mainly potassium (K) and chlorine (Cl), across the membrane. (Plonsey & Barr 2007). Around every organ there is also an electric field, generated by a monolayer of cells surrounding the organ. These transepithelial potentials are between 30 and 100 mV. Both membrane and transepithelial potential differences are generated and maintained by ion concentration gradients or constant flow of charged ions across the membranes or cell layers. (Nuccitelli 2011) Ion flows are generated most commonly voltage sensitive calcium (Ca^{2+}) channels, and pumps that are regulated by transcriptional, translational and gating mechanisms. In return, ion flows control the cell functions at the cell surface and in the cytoplasm. Many bioelectric signals can be produced and processes without modifying the mRNA but eventually these processes also change the gene expression. Bioelectric signals can act as major

regulators by activating downstream morphogenetic cascades via simple initial signal. (Levin 2011)

In a cellular level, when an electric field (dc or low-frequency ac) is applied in vitro or in vivo, several phenomena take place at the cellular level (Fig. 3); the membrane of the cathode-facing side of the cell is depolarized and the anode-facing side hyperpolarized. This leads to the activation of voltage-gated K^+ channels which stimulates integrin signals, or to opening of Ca^{2+} channels on cathode side and closing them on the anode side that leads to gradient of Ca^{2+}. This gradient can induce the release of Ca^{2+} from internal stores and there is in general an increase in cytosol calcium concentration which leads to actin cytoskeleton disassembly. Calcium concentration in cytosol in regulating cell proliferation, differentiation, cytoskeletal reorganization, gene expression and metabolism. Several cell type -dependent pathways are regulating the calcium oscillations; ion channels, phospholipase C (PLC), integrins and ATP all play a role in calcium dynamics in the cells. (Titushkin et al. 2011) PLC mediates the signaling through the release of internal Ca^{2+} and activation of protein kinase C which in turn couple to the mitogen kinase protein (MAP) kinase cascades. When PLC activity is blocked, calcium oscillations disappear. Calcium dynamics control also integrin-mediated cell adhesion and cell migration through phosphorylation of focal adhesion kinase (FAK). Integrins on the other hand, can regulate calcium dynamics, thus there is a correlation between focal adhesion formation and changes in Ca^{2+} dynamics. (Hart 2006) Applied electric field causes a reduction in the intracellular ATP levels which in return leads to the dissociation of actin cytoskeleton from the cell membrane as the ERM linker protein binding is inhibited. Growth factors bind to receptors that were redistributed due to the electric field and this triggers actin polymerization. Consequently, intracellular signaling pathways are activated. (Cho et al. 1994; I. Titushkin & Cho 2009; Titushkin et al. 2011)

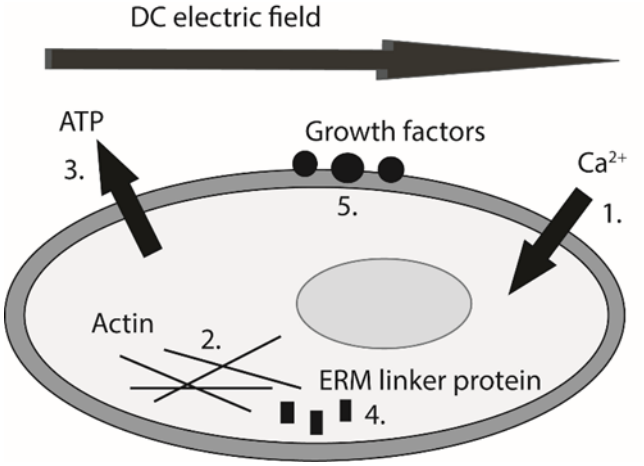

Figure 3. Schematic view of the effect of electric field on a cell and its calcium dynamics. Electric field increase the cytosol calcium concentration (1) which leads to actin cytoskeleton disassembly (2). The intracellular ATP levels decrease (3) which causes the dissociation of actin cytoskeleton from the cell membrane as the ERM linker protein binding is inhibited (4). Growth factors bind to receptors that were redistributed due to the electric field (5) and trigger actin polymerization. Modified from (Titushkin et al. 2011).

Bioelectric current signals are very different between regenerating and non-regenerating animals; for instance amputated salamander limbs maintain the direct current signal up to 100 mA/cm^2 whereas the current disappears slowly from the limbs that cannot regenerate. (Levin 2011) Also different cell types can have very different responses to electrical stimulation due to their distinct mechanical properties and receptor proteins at the plasma membrane (McCaig et al. 2009; Titushkin et al. 2004) or, in the case of neurons, for instance different developmental age or produced neurotransmitters (Rajnicek 2011).

1.3.1 Effect of endogenous and applied electric fields on the cell functions

Electric potentials and currents play a great role also in cell migration and orientation (Nuccitelli 1988), proliferation (Ross 1990), differentiation (Sauer et al. 1999), morphogenesis (Levin 2011), neuronal regeneration (McCaig et al. 1994), angiogenesis (Zhao et al. 2004), and wound healing (Cho 2002). Modulating

bioelectric fields can cause serious effects on developmental processes. (Nuccitelli 2011). The different effects of electric stimulus on the cell migration, orientation, adhesion and proliferation are discussed in the following subchapters and a short overview is given in the table 1. The stem cell differentiation is reviewed in the chapter 1.2.1.

Function	Cell type	EF threshold (mV/mm)	Reference
Migration	Endothelial	100	Li 2004, Zhao 2004
	Hippocampal	50	Rajnicek 2011
	Neurite	7	Rajnicek 2011
	Keratinocytes	5 – 400	Pullar 2011
Orientation	Endothelial	50 - 150	Zhao 2004, Bai 2004
	Hippocampal	28	Rajnicek 2011
Increased proliferation	Chondrocytes	150 – 300	Wang 2011
Decreased proliferation	Chondrocytes	450	Wang 2011
	HUVEC	200	Wang 2011

Table 1. The effect of the cell type and different stimulation parameters on the cell functions.

1.3.1.1 Effect of electric field on cell migration and adhesion

Several cell types, for instance neural crest cells, epithelial cells, keratinocytes, endothelial cells, fibroblasts, inflammatory cells and musculoskeletal cells show directional migration in the presence of a direct current electric field. The phenomena is called electrotaxis or galvanotaxis and it contributes into many physiological processes. (Gunja & Hung 2011) Most of the cell membrane proteins are negatively charged. In an external electric fields these proteins are pulled towards the positively charged anode. This phenomenon is called lateral electrophoresis. In electro-osmosis, sodium (Na^+) ions are accumulating near the negatively charged membrane and the Na^+ ions are pulled towards the negatively charged cathode in the external electric field. This creates a fluid flow very near to the cell surface and this flow is enough to pull also the membrane proteins towards the cathode. Usually both electrophoresis and electro-osmosis occur in the same cell membrane but the charge of the membrane surface, the charge and size of the membrane protein and its mobility in the membrane defines

which phenomenon dominates. (Rajnicek 2011) The response to electric field is nonlinear and strongly dependent on the cell type and the strength of the electric field. Some cells types migrate towards the cathode and some towards the anode. Even within the same cell type, migration direction can differ; endothelial cells isolated from big and small vessels migrate to different directions. (Wang et al. 2011) Usually the threshold for directional migration is around 100 mV/mm. (Li & Kolega 2002; Zhao et al. 2004) However, firing of hippocampal granule cells have shown to induce an electric field of 50 mV/mm that is enough to direct axonal projections. Neurites exposed to a DC field grow toward the cathode even at electric fields as small as 7 mV/mm and it was shown by culture medium prefusion that the directness is due to electric field itself rather than caused by gradients of tropic molecules. (Rajnicek 2011) Electromigration is an important factor for instance in wound healing. Endogenous electric fields that appear across the wound are in the range of 10 – 100 mV/mm. The center of the wound is more negative than the surrounding tissue that enhances the inflammatory cell and keratinocyte migration toward the wound site. Keratinocytes start responding already to electric fields of 5 mV/mm but the best respond is achieved with the fields between 100 and 400 mV/mm. With no electric field applied, keratinocytes migrate randomly on the substrate. When an electric field is applied to the keratinocyte culture in vivo, the cells start migrating towards the cathode. The migration starts within ten to fifteen minutes of field application and lasts until the field is removed. The wound closes up faster when a cathode is placed in the center of the wound. In contrary, when an anode was used, the keratinocytes migrated away from the wound center and the wound opened up. (Pullar 2011) Applied dc electric fields creating voltage gradients can be used in treating especially spinal cord injuries. Healing of the spinal cord is most probably due to regeneration of white matter, although this is difficult to test directly in humans. In a study with guinea pigs, a hollow silicon tube was placed in an injury site in the spinal cord and an electrode (cathode) was inserted in the middle of the tube. An electric field of around 2.5 mV/mm was produced inside the tube, and after one month it was shown that axons from both ends of the tube had started to grow toward each other inside the tube. Fine branches of regenerating axons were also found inside the astroglial scar within the injury. The effect of electric field was further enhanced when

neurotrophic factors were used. Generally, distally negative (cathodal) electric field enhance axonal migration and thus regeneration toward cathode but positive (anodal) electric fields direct axons away from the anode or cause more extensive dieback and resorption into the cell body. The used voltages range from a few mV/mm to hundreds of mV/mm. Clinical studies with human with spinal cord injuries showed that, in the best case, patients treated with oscillating dc electric fields gained back some motor or sensational function remarkably. (Borgens 2011)

Electric stimulation is also know to influence the cell adhesion. For example, direct currents increased stem cell adhesion to collagen gels (Sun et al. 2006), whereas fibroblasts and bone marrow osteoprogenitor cells exposed to direct or low frequency alternating currents resulted in cell detachment from culture plates (Blumenthal et al. 1997). Positively charged substrates and particles can also result in increase in cell adhesion, as demonstrated with melanoma cells. (McNamee et al. 2006)

1.3.1.2 Effect of electric field on cell orientation and elongation

Electric field stimulation have been shown to cause changes also in cell orientation and elongation. The cells usually align their long axis perpendicular to the electric field vector, perhaps in order to minimize the electric field gradient across the cell. (Gunja & Hung 2011) The cell alignment is seen both in actin filaments and microtubules. Cell orientation often occurs together with cell elongation. As cell migration, also orientation and elongation is dependent on the electric field strength and the stimulation time. With endothelial cells, field strength threshold was 50 – 150 mV/mm and 24 hour stimulation caused the orientation of the whole cell population. (Zhao et al. 2004; Bai et al. 2004) Hippocampal neurons have shown to align orthogonally in the dc electric field with fields as low as 28 mV/mm and there was also a decrease in the axons emerging from the cathode-facing sides of the somas and decrease in their axon length. The response to EFs differs between hippocampal axons and dendrites; growth cones of dendrites are attracted toward the cathode but those of axons are not influenced by the field. (Rajnicek 2011)

1.3.1.3 Effect of electric field on cell proliferation

Electric stimulation can both promote and inhibit cell proliferation, depending on the cell type and the field strength. Field strength of 150 – 300 mV/mm increase the proliferation of chondrocytes but decrease it with field strength of 450 mV/mm. (Wang et al. 2011) For HUVEC cells, field strength of 50 – 100 mV/mm does not change the proliferation rates but already 200 mV/mm decrease the proliferation. The same applies for ocular lense epithelial cells. (Wang et al. 2003; Wang et al. 2005) PI3K/Akt signaling pathway is related to both apoptosis and proliferation. It is know that electric field stimulation activates this signaling pathway and thus decreases the apoptosis rate and increases the proliferation of the cells. An ischemic brain tissue was stimulated with electric field and there was a significantly smaller number of apoptotic cells, and this effect disappeared when PI3K/Akt signaling was blocked. (Wang et al. 2011)

1.3.2 Methods for applying the electrical stimulation

Cells and tissues can be exposed to electrical stimulation by using specific stimulation devices. Common features to all of them are a biocompatible stimulation chamber, incubator compatibility and working as a closed circuit system providing voltages of a physiological range. The devices can also be designed to protect the samples from unwanted electric sources. Direct current stimulation devices often use electrochemical cells called salt bridges to prevent cytotoxic redox reactions in the actual stimulation chamber where the cells or tissues are located. In the case of alternating current, either capacitively coupled or inductively coupled devices are used. Capacitively coupled devices consist of electrode plates that generate an electric field between them and are not in contact with the cell culture medium. In inductively coupled devices, the electrodes are in direct contact with the medium and they transfer the electric current to ionic current at the electrode-electrolyte interface. The electrodes are chosen based on their characteristics, such as biocompatibility, corrosiveness, charge transfer and cost. Often used electrode materials are for instance silver/silver chloride, platinum, gold, titanium and stainless steel alloys. (Hronik-tupaj & Kaplan 2012)

The most important parameter in electrical stimulation is the level and nature of the electric voltage or current applied. Effects on cells, such as increased proliferation, take place with both relatively high and low currents and voltages and the most limiting factor is a certain threshold above which the cell death starts to occur. Often a steady dc currents and voltages are being used but there also studies done for instance with pulsed dc and ac of different frequencies. Often the best results are achieved with frequencies less than 100 kHz which is also the frequency range for electric fields occurring in vivo. (Balint et al. 2013) In general, dc field stimulation is typically used for controlling cell orientation, morphology and migration whereas ac field stimulation has shown to enhance cell differentiation and increase tissue function. (Hronik-tupaj & Kaplan 2012)

1.3.3 How the cells sense the electricity

It has been shown in several experiments that cells are able to sense and transduce electric fields but the actual mechanism is still partly unknown. The cells could either sense the electric field directly, or they could sense for instance the increase in growth factor secretion caused by the electric field. Small applied potentials cannot penetrate the cell so the electric field influences the plasma membrane itself or its proteins. The possible effects could be; perturbation of the membrane potential, redistribution of charged membrane components, or interplay between signaling mechanisms. It should also be considered that the electric field the cell is actually experiencing, is not the same than the field applied to the system. Often it is reported that the field the cell is sensing is simply the applied voltage divided by the electrode separation. At dc and low-frequency electric fields (below 1 MHz), cell plasma membrane works as relatively good insulator so the transcellular voltage gradient cannot penetrate into the cytoplasm but would stay extracellular and the cytoplasmic electric field can be considered as negligible compared to the external field. If the cell concentration is low, one can use only the medium conductivity in the calculations but if the cell concentration is high, one cannot ignore the insulating effect of the cells that is decreasing the total conductivity and also the transmembrane potential difference (ΔV) of individual cells. In that case, ΔV has to be expressed in terms of the volume fraction of the cells. ΔV and the electric

field at the cell surface (Es) are also different depending whether the cells are plated on a substrate or in a suspension. Generally, the variation in these two parameters should be always taken into consideration when interpreting the experimental results. (Rajnicek 2011; Hart 2011)

There are few prerequisites for the experimental (and simulation) conditions. The applied electric field is assumed to be uniform so the cell must be much smaller than the measurement chamber and it should not be located near the electrodes or chamber walls. The conductivity of the medium should be more or less the same as that of the cytoplasm (around 1 S/m), otherwise the expression for ΔV becomes more complicated as the transmembrane conductivity can no longer be neglected. If low-conductivity medium is used, one has to define ΔV as a function of membrane and cytoplasmic conductivity as well. Also the cell shape has to be taken into account when defining ΔV; it is usually higher for random shaped than for symmetric cells. (Hart 2011)

Besides sensing the electric field directly, as described above, the cell might also sense for instance the increase in growth factor secretion caused by the electric field. There are two major molecular mediators that are altered during the electrical stimulation, Ca^{2+} and ATP. There is probably no predominant electric field membrane receptor but there are several transmembrane proteins that might be involved in sensing and responding in electric field. The following transmembrane proteins might be involved for instance in cathodal steering of the cells; nerve growth receptor, brain-derived neurotrophic factor receptor, cannabinoid receptor and voltage-gated Ca^{2+} channels. (Titushkin et al. 2011) Inhibiting the VEGF receptors cancels the electric field effect on cell orientation and elongation. (Zhao et al. 2004) When using voltages above 200 mV/mm, electric stimulation alters the membrane potential but even with small stimulation voltages (10 mV/mm) that cannot change the cell membrane potential nor activate VGCCs, cells still sense and respond to electrical stimulus. This might be due to the fact that with this small potentials, exposure times needed (> 1h) (Khatib et al. 2004) might be long enough to induce cellular responses via mechanisms other than direct changes in calcium, such as cell surface receptor redistribution. (Titushkin et al. 2011) Ligand-receptors interactions and subsequent cytoplasmic signaling are biased

cathodally and cathode becomes analogous to a chemoattractant. Also, cell orientation has been seen also in the absence of extracellular Ca^{2+} or cytoplasmic Ca^{2+} gradients, however it is possible that cell adapt to the low Ca^{2+} levels and start using other signals to maintain the orientation. (Rajnicek 2011) High frequency alternating electric fields on the other hand are able to penetrate inside the cell and can possibly influence directly the intracellular processes. (Titushkin et al. 2011)

1.3.4 Cell electric impedance

At the frequency range of few hundred kilohertz, so-called β-dispersion region, cell membrane of the intact cells becomes polarized and can be modeled as a capacitor in series with a resistor that corresponds the electrolyte inside and outside the cell. (Davey et al. 1998, Giaver et al. 1986, Pliquett et al. 2009) Contrary to higher frequencies, cells behave as insulating particles; thus, the current bypasses the cells and impedance of the whole system is increased. (Arndt et al. 2004) Damaged membranes of dead cells allow ions to leak and do not resist current flow. (Markx et al. 1999) It is possible to evaluate cells as well as cell-scaffold constructs noninvasively and repeatedly by means of their dielectric properties.(Bagnaninchi et al. 2011, Markx et al. 1999) Impedance and dielectric spectroscopy that both measure the impedance spectrum of a sample have been utilized in studying cells cultured directly on the electrodes, (Bagnaninchi et al. 2011, Markx et al. 1999) or nonivasively, (Savolainen et al. 2011) and to some extent also cells in 3D structures, where measurement probe was used. (Bagnaninchi 2004, Dziong 2007) The change in impedance is associated with an increase in a volume fraction of cells in suspension, change in cell physiology or a cell type. The complex impedance is measured at multiple frequencies and the method can be used in monitoring cell suspensions or 3D scaffolds or gels. Nevertheless, it has also been observed that the increase of the cell number can be seen as a decrease of the real part of the impedance. (Bagnaninchi et al. 2010)

1.4 Electrochemistry

The electric current flows as charges that are carried by electrons at the electrode and by ions in electrolytes (solutions of acids, bases and salts). At electrode/electrolyte interface, electrochemical reactions are necessary for exchanging electrons to ions (Fig. 4) Oxidation reactions take place in the anode and reduction reactions at the cathode. (Plonsey & Barr 2007)

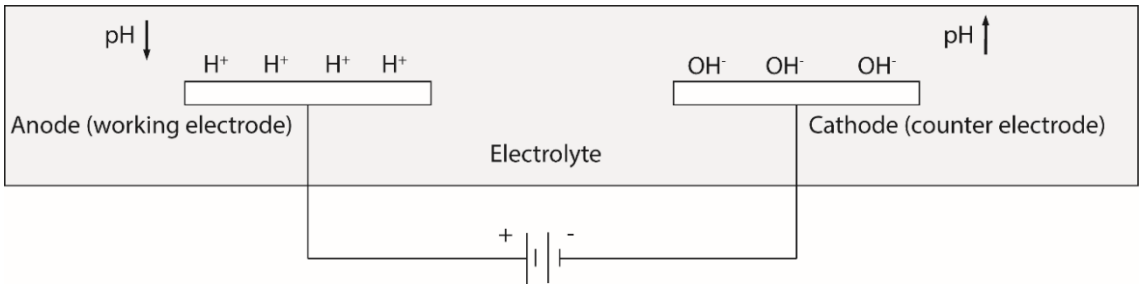

Figure 4. The electrode setup and the oxidation/reductions reactions and consequent changes in pH at anode and cathode.

When cells or tissues are stimulated with electrodes in an aqueous physiological medium containing sodium chloride (NaCl), several electrochemical reactions take place at the electrode/electrolyte interface in order to change the electrons carrying the current in the electrode for ions carrying the current in the electrolyte. These reactions produce electrochemical products and can also affect the electrode itself. The reactions taking place at the capacitive region (Fig. 5) are completely reversible, and electrochemical reactions occur right from point I (oxidation) or left from point II (reduction). The electrochemical reactions can be reversible or irreversible, depending whether the products remain at the electrode or diffuse away. The voltage limits for the reactions are dependent on the electrode material and the capacitive region can be expanded for instance by increasing the electrode surface area or coating the electrode with an insulating film. (Plonsey & Barr 2007)

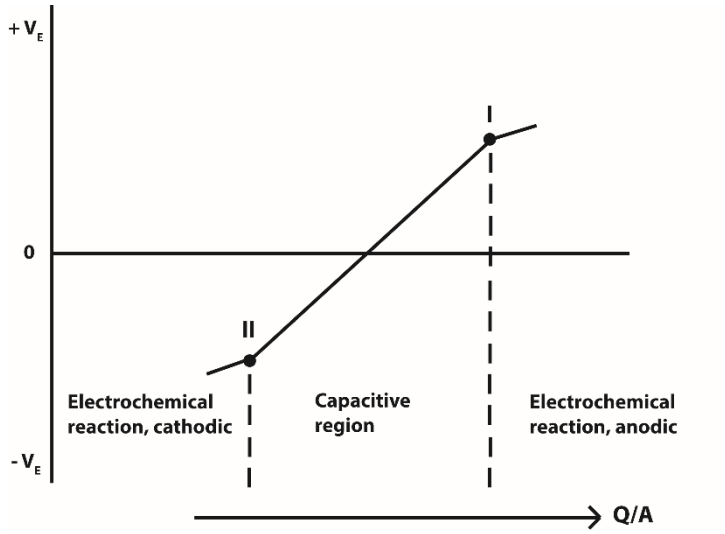

Figure 5. Relationship between electric potential and charge density. Processes at the capacitive region are completely reversible. Electrochemical reactions take place right from the point I and left from the point II and are either reversible or irreversible. Irreversible reactions result in diffusion of new species to the electrolyte. Modified from (Plonsey & Barr 2007)

The main reactions taking place at the electrode/electrolyte interface are:

Reactions at the cathode

$$2H_2O + 2e^- \leftrightarrow H_2 + 2OH^- \qquad E^0 = -0.83\,V \quad (1)$$

$$Na^+ + 1e^- \leftrightarrow Na \qquad E^0 = -2.71\,V \quad (2)$$

Reactions at the anode

$$2H_2O \leftrightarrow O_2 + 4H^+ + 4e^- \qquad E^0 = 1.23\,V \quad (3)$$

$$2Cl^- \leftrightarrow Cl_2 + 2e^- \qquad E^0 = 1.36\,V \quad (4)$$

At the cathode, reaction 1 leads to an increase in pH in the close vicinity to the electrode. At the anode, the oxidation of water (reaction 3) leads to a decrease in pH. Gabi et al (Gabi et al. 2009) have modeled the changes in pH at the electrodes and also showed that these changes can influence the cell viability. Cell viability is also

affected when reaction 4 occurs as it generates toxic amounts of hypochloric acid. Also other chemical compounds can be generated depending on the electrode material and the used voltage. Platinum electrodes do not create reduction/oxidation (redox) species but for instance stainless steel, indium tin oxide (ITO) and copper do. Stainless steel contains iron, carbon and chromium and sometimes also for instance nickel and titanium. Chromium forms together with oxygen a protective, passive film but the chlorides in the electrolyte can destroy the film and generate for instance Fe^{2+} ions. In the case of copper electrodes, Cu^{2+} ions are being produced. Thus, when applying electric currents to cells, one has to take into account both the changes in pH and the products of electrochemical reactions in respect to cell viability.

1.5 Tissue engineering

The ultimate goal in tissue engineering is to engineer an entire functioning organ. This requires mimicking the complex natural organization and both living cells and engineered materials have to be used without forgetting the external biological, mechanical and chemical cues. The ideal cell source would be the patient`s own cells as they do not cause any immune reactions. Mature cells do not proliferate fast enough, or at all, and they are also usually very scarce, thus using the adult stem cells of the patient could offer a solution. Other cell types suitable for tissue engineered application are embryonic or induced pluripotent stem cells. In addition to choosing the suitable cells, they need to be provided a tailored environment that triggers them to form the desired tissue or organ. One factor is the biomaterial, namely scaffold where the cells are seeded in. They have to mimic the natural topography and other characteristics of the tissue. In addition, the scaffold-cells construct has be cultured under the proper environmental cues. (Khademhosseini et al. 2009)

2. Aim of the work

The first goal of this thesis was to study if the cell number in a biomaterial scaffold can be quantified by measuring the impedance of the scaffold-cell constructs. The work, presented in publication I, was performed in Tampere University of Technology, Finland and later, the research was moved to the Laboratory of Biosensors and Bioelectronics (LBB) at the ETH Zürich, Switzerland. The research done at the ETH was initially based on the previous study conducted at the LBB about the effect of applied current on the cell viability and adhesion. The idea was to extent the study from the two-dimensional substrates to the three-dimensional scaffolds and to control the migration and adhesion of the cells into the scaffold by applied electric current. The aim was to provide an alternative method to asymmetric scaffold design, and construct complex tissue-engineered structures, combining more than one cell type within the same construct.

The initial findings from the cell stimulation by applied electric current led to a new project; inducing the neural differentiation of adipose-derived stem cells by electric field and copper. Adipose-derived stem cells have a multilineage potential and they are also easy to harvest, compared to many other stem cell types. The adipose-derived stem cells could provide an autologous source for the next generation neural regeneration. Inducing the differentiation by electric field and copper may offer a novel, growth factor-free approach for the neural differentiation of stem cells.

In addition to the washing assays performed in the previous projects, the actual adhesion forces were further quantified with a technology called FluidFM. Apart from the standard staining protocols and washing assays used to investigate cell viability, cellular structure, and adhesion, a quantitative method based on the FluidFM was used for the first time to study the effect of electric stimulation on the cell adhesion forces. FluidFM provided a fast, serial single-cell measurements and the adhesion forces could be measured up to the µN range, which is not possible with any other method.

3. Materials and methods

3.1. Cell cultures

Two different cell types were used in this thesis; human adipose-derived stem cells (ADSC) and mouse myoblasts (C2C12). The C2C12 cells were obtained from the American Type Cell Collection and the ADSCs were isolated from adipose tissue samples collected from the subcutis/pelvic region or breast of female patients (n = 3, age = 52 ± 12 years) undergoing elective surgical procedures in the Department of Plastic Surgery at Tampere University Hospital (Tampere, Finland). The human ADSCs were isolated and characterized at passage 5-6 by FACS using lineage-specific markers as described previously (Lindroos et al. 2009). Shortly, the adipose tissue was minced manually into small fragments and digested with 1.5 mg/mL collagenase type I (Life technologies, Paisley, UK). The digested tissue was centrifuged and filtered to separate the ADSC from the surrounding tissue. The isolated cells were then expanded in Dulbecco`s modified Eagle medium (DMEM/F-12 1:1) supplemented with 1% Glutamax I, 1% antibiotics/antimycotic and serum from 10% fetal bovine serum (FBS), all purchased from Life technologies, Paisley, UK. Cultured ADSCs at passages 3-5 (n=4) were analyzed with monoclonal antibodies with flow cytometry (FACSAria; BD Biosciences, Erembodegem, Belgium). Monoclonal antibodies against CD14-PE-Cy7, CD19-PE-Cy7, CD45RO-APC, CD49D-PE, CD73-PE, CD90-APC, CD106-PE-Cy5 (BD Biosciences Pharmingen); CD34-APC, HLA-ABC-PE, HLA-DR-PE (Immunotools GmbH Friesoythe, Germany); and CD105-PE (R&D Systems Inc, MN, USA) were used. Analysis was performed on 10000 cells per sample, and the positive expression was defined as the level of fluorescence 99 % greater than the corresponding unstained cell sample.

All the experiments were done in 37 °C and 5 % of CO2 unless otherwise stated. C2C12s up to the passage 25 were cultured in Dulbecco's modified Eagle's medium (DMEM) supplemented with 10% FBS and 1% antibiotic-antimycotic (all from Thermo Fisher Scientific AG, Switzerland). ADSCs were cultured to passage 5 or 6 in DMEM/F-

12 supplemented with 10% heat-inactivated fetal bovine serum (FBS), 1% glutamax and 1% penicillin-streptomycin (all from Thermo Fisher Scientific AG, Switzerland).

3.2 Experimental setups

The setup for cell impedance measurements presented in the chapter 3.2.1 was used in the publication I. The setups for measuring cell proliferation, morphology, viability and adhesion, presented in the chapter 3.2.2 are used in publications III and IV. The two setups for studying neuronal differentiation, presented in the chapter 3.2.3 are used in the publication II.

3.2.1 Cell impedance measurements

The electric impedance of cells was measured in order detect the existence and number of viable cells inside a three-dimensional scaffold based on their dielectric properties. The scaffolds were PLA 96/4 scaffolds, made of medical grade, highly purified poly-L,D-lactide 96/4 (PLA 96/4) with an inherent viscosity of 5.48 dl/g (Purac Biochem BV, Groninchem, The Netherlands). The scaffolds were prepared from 125 mm long piece of PLA96/4 knit by rolling it to a cylinder with diameter 10 mm and height 8 mm. The roll was fixed with a droplet of highly viscose PLA dissolved in acetone and allowed to evaporate.

After pre-incubation of the scaffolds in the cell culture medium for 3 days, scaffolds were placed on non-adherent 24-well cell culture plates (Nunclon^{TM}Δ Surface, Nunc^{TM}, Roskilde, Denmark) and seeded with 10^4, 10^5 or 10^6 ADSCs. Cells were allowed to adhere for 3 hours in the cell incubator and 500 µl media was then added to each of the wells. Scaffolds without cells were maintained in the medium for 3 weeks and impedance was measured at day 1, 7, 14, and 21. In addition, the ADSC-seeded scaffolds were measured at the same time points. Culture media were changed at 3-day intervals and impedance was measured 2 hours after the change. Prior to the measurements, scaffolds were moved with sterile tweezers from the well plates to a fertilization dish (BD, Franklin Lakes, NJ, USA) that was filled with 3 ml of medium.

Measurements were performed using a Biopac MP35 and Electrical Bioimpedance Amplifier EBI100C (Biopac Systems Inc., Goleta, CA, USA). Four T-shaped working electrodes made of 99.9% pure silver were aligned in the cover of the fertilization dish (Fig. 6). A four-electrode system was used, in which the two outer electrodes fed current to the system and the two inner electrodes measured the voltage. Both the scaffold and the electrodes were in direct contact with the cell culture medium. Small (400 µA) current was supplied at a frequency of 100 kHz and the real part of impedance, i.e. the resistance was measured. The real part of the impedance of the both media was measured prior each measurement and subtracted from the values of the measured scaffolds to cancel the effect of the medium impedance. Values are presented as relative %-difference compared to the 1-day scaffold.

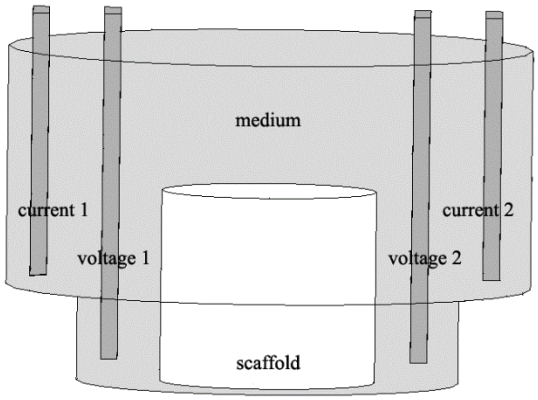

Figure 6. Measurement configuration of the dish, scaffold and electrodes. Distance from the scaffold to the current feeding electrodes was 4 mm and to the voltage measurement electrodes 10 mm. Electrode width was 4 mm and a gauge 1 mm. Electrodes were 1 mm distance from the bottom of the dish.

3.2.2 Cell proliferation, morphology, viability and adhesion

The effect of applied electric current on the cell proliferation was studied with the ADSCs either seeded on a glass slide or in suspension, subjected to an electric current or additionally also to small amounts of Cu^{2+} released from the stimulating electrodes by electrolysis. The number of cells on day 4, 7, and 14 was counted and compared to the cell number at the day 4 control unless otherwise stated. The experimental setup is

the same as for the neuronal differentiation and is described in more detail in chapter 3.2.3. The same setups were used to study the viability and morphological changes of the ADSCs.

The viability, morphology and adhesion of C2C12s were studied with the setups consisting of indium tin oxide (ITO) coated glass slides (MicroVacuum Ltd., Hungary) mounted into custom-made chambers of poly(methyl methacrylate) base and polytetrafluoroethylene housing. Two different types of chambers and ITO electrodes were used for the experiments (Fig. 7). Chambers were cleaned for 10 min in 70% ethanol, rinsed with Milli-Q water, then left in a laminar flow hood to dry until the ITO was cleaned in 2% sodium dodecyl sulfate (SDS) for 20 min and rinsed with Milli-Q water, followed by blow drying with nitrogen gas and 2 min plasma cleaning in oxygen atmosphere. Prior to the experiments, chambers were incubated with cell culture medium for 20 min, followed by seeding of 60 000 and 20 000 cells/cm^2 in the small and big chambers, respectively. Cells were incubated for at least two hours before the electrical stimulation was started. As external stimuli, anodic, pulsed monophasic currents were applied to the ITO working electrodes using an Autolab PGSTAT 302N potentiostat/galvanostat (Metrohm Autolab B.V., Netherlands). An alternating current on and off periods were both 5 seconds long, with an applied current density of 0.01 and 0.03 A/m^2. Current doses (As/m^2) were calculated from the total current on time for each current density.

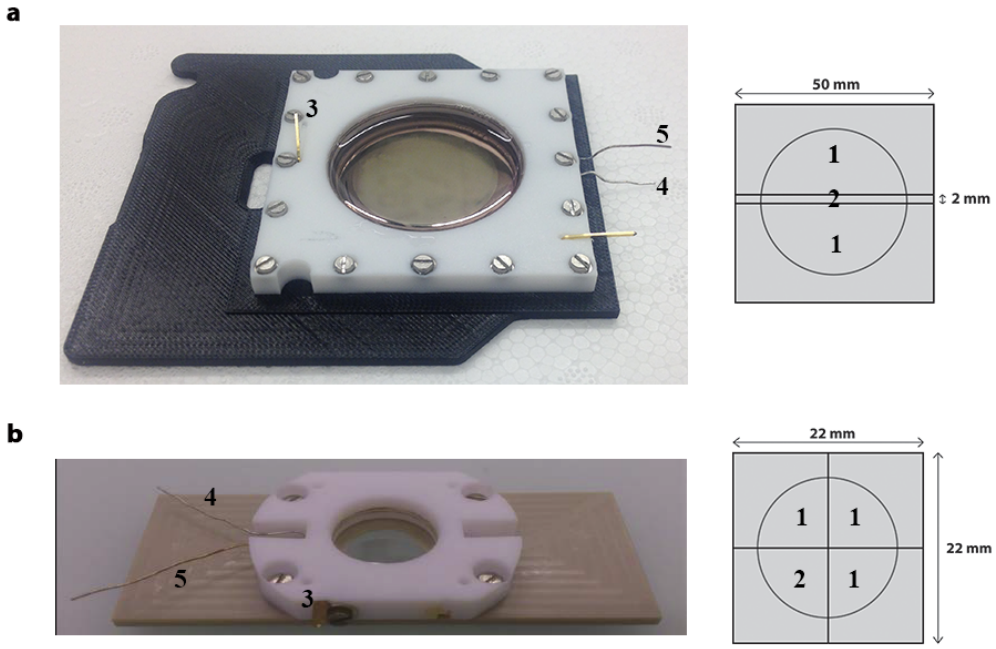

Figure 7. Chamber and ITO electrode configurations for adhesion force measurements (a), and viability and focal adhesion assays (b). The ITO surface consisted of isolated control areas (1) and a working electrode (2) connected to a potentiostat through copper pins (3). Platinum (4) and silver wires served as counter (4) and reference (5) electrodes, respectively.

Cell adhesion and migration to three-dimensional scaffolds was studied with a setup that used a non-conductive non-woven PLA 96/4 scaffold with a thickness of approximately 2 mm. The scaffold was surrounded by two conductive metallic meshes. The scaffold and meshes were housed by a polyether ether ketone (PEEK) plastic frame (Fig. 8) The meshes, the plastic frame and the electrode configuration are described in more detail in the chapter 3.2.3. The scaffold and meshes were disinfected in 70% ethanol and incubated first in phosphate buffered saline (PBS) and then in cell culture medium for one hour prior to fitting them inside the frame that was tightly closed. Approximately 2 000 000 cells in a total volume of 10 ml were seeded in a falcon tube that housed the mesh-scaffold construct and the whole tube was placed in a magnetic stirrer that provided a continuous mixing of the cell suspension.

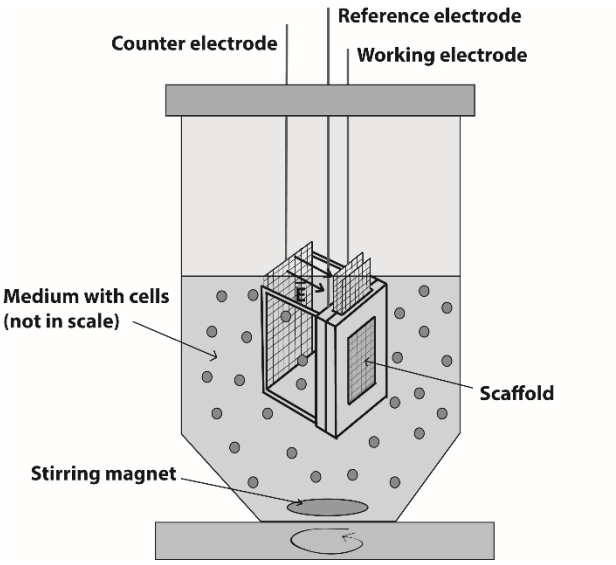

Figure 8. PLA scaffold and two metallic meshes surrounding the scaffold were housed in a plastic frame. One of the meshes served as working electrode. Counter electrode, made from the same material as the working electrode, was placed 10 mm apart from the working electrode. Platinum wire was used as a reference electrode. The direction of the electric field is indicated by arrows.

A monophasic pulsed current (current 5 seconds on, 20 seconds off) was applied for one hour with a PG580 potentiostat/galvanostat (Princeton Applied Research, TN, USA) in galvanostatic mode. A pulsed dc current was used to minimize the damage to the electrodes and the electrochemical generation of toxic species. Current densities of 1, 4, and 6 A/m^2 were used and the cell migration and adhesion into the scaffold was compared to the control condition applied without current.

3.2.3 Neuronal differentiation

Two different experimental setups were used when studying the neuronal differentiation of ADSCs stimulated with Cu^{2+} and/or electric current (Fig. 9). The stimulation chamber for adhered cells consisted of the stimulation electrodes and a polydimethylsiloxane (PDMS) chamber that housed the cell culture medium. Sylgard® 184 Silicone Elastomer kit (Dow Corning, USA) was used to make the PDMS chamber. The ratio between the base and curing agent was 10:1. The PDMS was cured at 80 °C

for at least 2 hours. The cells were seeded on a glass slide that was placed between the working and the counter electrodes inside the PDMS chamber. The counter and working electrodes were made of either copper or platinum and they were connected to the current source outside the cell chamber. A silver wire served as a reference electrode. The area of the glass slide was 4.2 cm^2 and the distance between the working and counter electrode was 1.4 cm. The setup allowed for replacing the electrodes in case they got damaged or needed to be changed to another material. (Fig. 9 A) Prior to the stimulation, the cells were plated on the glass slides with the cell density of 3 000 cells/cm^2.

The experimental setup for stimulating the cells in suspension consisted of the stimulation electrodes that were housed by a PEEK plastic frame. The working and counter electrodes were stainless steel square weave meshes (G Popp&Co AG, Zurich, Switzerland) that were further modified by C. Jentner Oberflächen- und Galvanotechnik (Pforzheim, Germany) by first coating them with copper. Copper was then coated with a very thin layer (approximately 0.2 µm) of palladium to enable the platinum coating (thickness of 1 µm) on the uppermost layer of the mesh. The surface area of the electrode was 2.6 cm^2. Due to the cutting of the electrodes to the desired size, the copper was exposed on the electrode edges. When the cells were stimulated with electric current only, 99.9 % platinum electrodes were used as both working and counter electrodes. The distance between the working and counter electrode was 10 mm. A silver wire was used as a reference electrode. The plastic frame-electrode construction was placed in a 50 ml falcon tube where 1.5 – 2 million cells were seeded in the total volume of 10 ml. The tube was placed in a magnetic stirrer that provided a continuous mixing of the cell suspension. (Fig. 9 B)

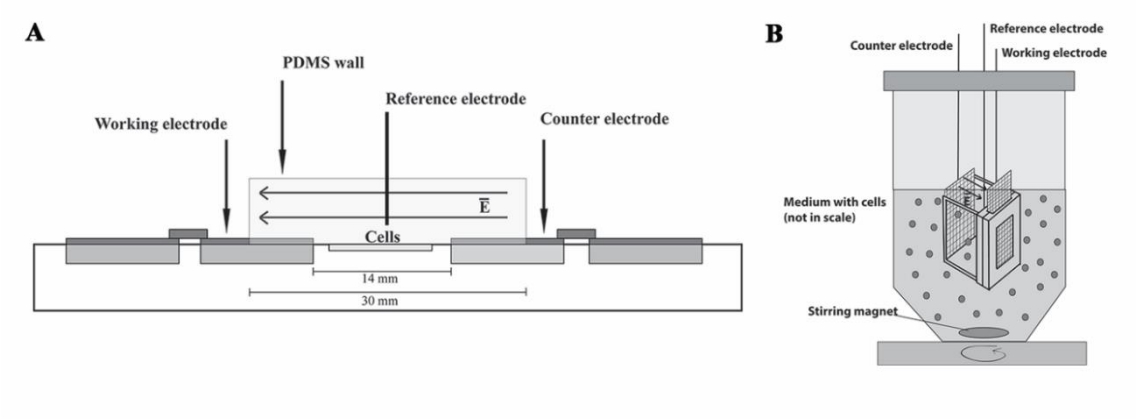

Figure 9 Experimental setups for the neuronal differentiation of adhered cells (A) and cells in suspension (B).

In both experimental setups several different current densities and copper amounts were tested both alone and together. When the current was applied via copper-containing electrodes, the copper (Cu^{2+}) was released gradually to the cells through electrolysis and the cells were thus stimulated with both current and gradually released Cu^{2+}. In current only stimulation, current was applied through platinum electrodes and no Cu^{2+} was released to the cells. For all of the stimulations with a current, a monophasic pulsed current (current 5 seconds on, 20 seconds off) was applied for one hour. In experiments with cells in suspension, a PG580 potentiostat/galvanostat (Princeton Applied Research, TN, USA) and in experiments with adhered cells, an Autolab potentiostat (Methrom Autolab, Utrecht, Netherlands), both used in galvanostatic mode. The electric field E= U/d was 35 mV/mm for the current of 1 mA and 53 mV/mm for the current of 1.5 mA when copper-containing electrodes were used, and 155 mV/mm for the current of 1 mA when platinum electrodes were used.

In copper only stimulation, Cu^{2+} was first released into the medium from the copper electrode via electrolysis in the absence of cells, and the Cu^{2+}-containing medium was then collected and added to the cell suspension all at once (abrupt release). For the adhered cells, several different current magnitudes and thus Cu^{2+} amounts were used, for the cells in suspension, Cu^{2+} was released only with the current of 1 mA.

The mass of the Cu^{2+} released by electrolysis is calculated by using Faraday`s laws of electrolysis $m = \frac{Q}{F} * \frac{M}{z}$ where m is the mass of the released Cu^{2+}, Q is the total electric charge passed through the electrode, M is the molar mass of Cu^{2+} and z is the number of electrons transferred per ion. In addition, the mass of released Cu^{2+} was measured by weighing the electrodes before and after the experiment.

The different stimulation conditions are presented in the table 2.

Condition	Current (mA)	Copper (µg/ml)	Copper release
Adhered cells	1, 1.5, 2	24, 36, 48	Gradual
Adhered cells	1, 1.5	-	-
Adhered cells	-	6 - 36	Abrupt
Cells in suspension	1	24, 36	Gradual
Cells in suspension	1, 1.5	-	-
Cells in suspension	-	24	Abrupt

Table 2. ADSCs in suspension or adhered on the substrate were stimulated either with copper, current or both of them.

After the 1 hour stimulation of cells in suspension, cells and the medium were collected and 4 000, 3 000 or 2 000 cells were seeded in chamber slides for 4, 7, and 14 days immunohistochemical analysis, respectively. Rest of the cells were seeded in culture flasks (real-time PCR and western blotting) and cultured for 4, 7, or 14 days as well. At day 3, medium still containing Cu^{2+} from the stimulation, was exchanged with the control culture medium, namely DMEM/F-12 supplemented with 20% heat-inactivated FBS, 1% glutamax and 1% penicillin-streptomycin in all experimental conditions. Later, medium was changed every three days. In the studies with adhered cells, the cells on the glass slides were analyzed at day 7 with immunostaining.

3.3 Methods

The cyclic voltammetry described in the chapter 3.3.1 was used to assess the electrode materials used in the publications II, III, and IV. The Fluidic Force Microscopy

technique described in the chapter 3.3.2 was used to quantify the cell adhesion forces in the publication IV. The cell analysis methods presented in the chapter 3.3.4 were used in all the publications. In more detail, the semiquantitative measurement of DNA was used in the publication I and the viability staining in the publications II, III, and IV. The immunofluorescent staining for focal adhesions was used in the publication IV and for protein specific for neurons in the publication II. Real-time PCR and western blot were used in the publication II.

3.3.1 Cyclic voltammetry

Cyclic voltammetry was used to determine the safe limits for the electrical currents and potentials that could be applied to the electrodes without causing damage to them due to oxidation and reduction processes. The cycling scan over a defined potential interval was performed and the resulting current was recorded and plotted against the potential. The positive current peak indicates the reduction reaction and negative current peak the oxidation reaction. Cyclic voltammetry was performed for ITO electrodes and stainless steel electrodes with and without platinum coating in cell culture medium.

3.3.2 Fluidic Force Microscopy (FluidFM)

The cell-substrate adhesion forces were measured with a technique called Fluidic Force Microscopy (FluidFM) that combines atomic force microscopy (AFM) with microfluidics. AFM can be used for force spectroscopy where the object is scanned with the cantilever and the forces affecting the cantilever cause it to bend. The bend is measured via the reflection of the laser from the cantilever to the photodetector. (Fig. 10)

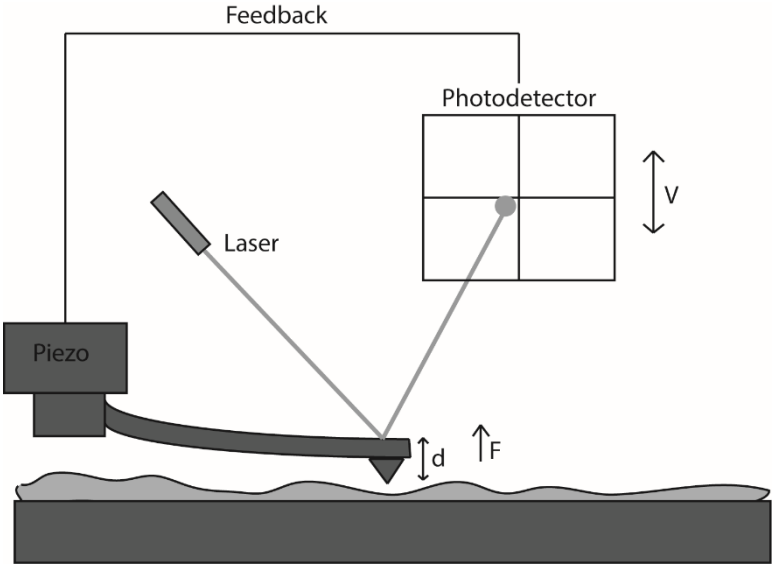

Figure 10. The working principle of the AFM. Forces affecting the cantilever cause it to bend (deflection [d]) which is seen as change in the reflected laser signal on the photodetector. This change can be measured as change in voltage (V) that can be translated to force (F). The piezo and feedback system allow the vertical tip position control.

Due to a microchannel integrated in the cantilever, FluidFM allows for measuring the force-distance curves for a cell immobilized to the cantilever via pressure applied through the microchannel. A FluidFM system (Cytosurge AG, Zürich, Switzerland) can be mounted on top of a microscope, in this case on an Axio Observer.Z1 inverted microscope (Zeiss, Feldbach, Switzerland). The sample chamber was placed on a 100 µm piezoelectric Z-stage. A hollow cantilever with a microfluidic channel was mounted on the scan head and connected to a digital pressure controller (Cytosurge AG). The cantilevers were rectangular, tipless silicon nitride probes coated with gold to obtain a good reflected laser signal on the AFM photo detector. The aperture of the cantilevers was 8 µm in diameter, large enough to apply enough force to detach the cell from the substrate without damaging the cell membrane, but small enough to be entirely positioned on an adhered cell.

Before starting to use a new cantilever, it was calibrated for the spring constant (k [N/m]) based on the theory of Sader et al. (Sader et al. 1999) Prior to each experiment, the cantilever was filled with MilliQ water by applying an overpressure until the liquid reached the aperture. In addition, the sensitivity of the cantilever was measured by performing force spectroscopy on a cell-free area on the substrate. Sensitivity (S [V/nm]) translates the photo detector signal (V [volts]) into the bending of the cantilever [nm], and the force (F) is derived by F= V/S*k.

During the cell adhesion measurements, the cells seeded in the measurement chamber were approached in contact mode with a set point of 5 nN and a speed of 1 µm/s. Once the cantilever was brought into contact with the cell, an under-pressure of 800 mbar was applied. After 10 s, enough for the establishment of the contact between the probe and the cell, the probe was retracted with the same speed, while the pressure was maintained and the deflection signal of the probe was recorded until the cell had completely detached from the surface. As the last step, an overpressure of 1000 mbar was applied to prevent further adhesion of the cell on and in the probe. The working principle of the FluidFM is presented in the figure 11.

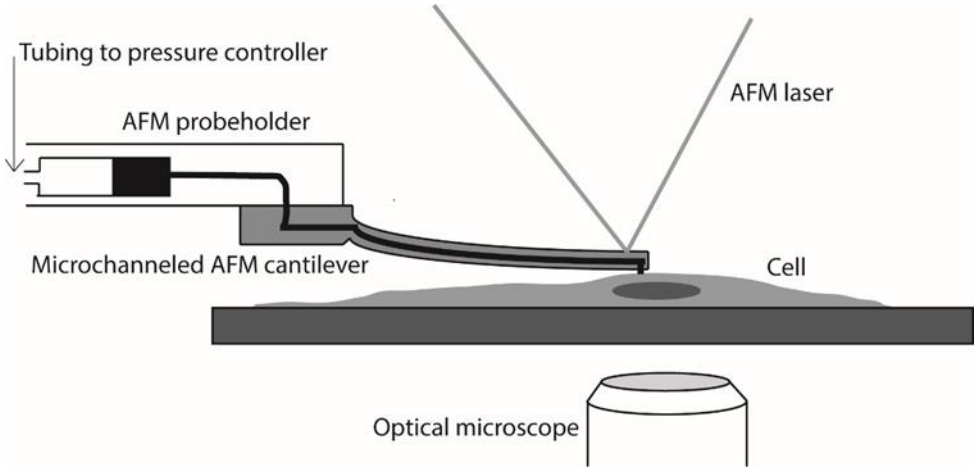

Figure 11. The schematic of the FluidFM setup. The cell is immobilized to the cantilever by applying a pressure via the fluidic microchannel. The deflection of the cantilever due to the approach to and detachment of the cell enables the measurement

of the resulting force-distance curve. The whole process can be visualized with an optical microscope.

After each adhesion force measurement, the cell culture chamber was quickly replaced by containers of cleaning solutions without removing the cantilever from the scan head. The cantilevers were cleaned by first dipping them in 5 % sodium hypochlorite and then thrice in Milli-Q water. After the experiments, the cantilevers were stored in Milli-Q water supplement with 2 % antibiotic-antimycotic (Thermo Fisher). As a result of the cleaning, single cantilevers could be typically used for 10-50 measurement cycles unless they got mechanically damaged.

3.3.3 Cleaning protocols

In the neuronal differentiation and cell adhesion studies, all the electrodes, the plastic and PDMS parts and the glass slides were first cleaned with 2 % sodium dodecyl sulfate (SDS) for 20 min and rinsed with Milli-Q water followed by blow drying with N_2. Prior to the cell seeding, the ITO and glass slides where the cells were directly adhering, were cleaned 2 min in oxygen plasma. The plastic parts were cleaned for 10 min in 70 % ethanol, rinsed with Milli-Q water and then let to dry inside the laminar hood.

In the cell migration and adhesion studies into a scaffold, the PLA scaffold was disinfected in 70 % ethanol and then incubated first in PBS and then in cell culture medium for one hour.

3.3.4. Cell analysis

3.3.4.1 Cell number and viability

Cell number was measured prior to each experiment with Countess® Automated Cell Counter (Thermo Fisher). In addition, in the experiment of cell migration and adhesion into the scaffold also the cell size was measured with the same device.

Cell viability in the adhesion experiments in 2D and 3D, and neuronal differentiation experiments of adhered cells was visualized by fluorescent live/dead staining after 1 hour exposure to the current and in control condition without current. The electrodes or

the scaffold with cells were rinsed once with PBS and incubated with a mixture of 1 μM calcein AM and 3 μM ethidium homodimer-1 (Molecular Probes™, Life Technologies, Zug, Switzerland) for live and dead cells, respectively. After 45 min incubation, the probe solution was replaced with cell culture medium.

3.3.4.2 Immunofluorescent staining

Immunofluorescent staining was used for visualizing the focal adhesion when studying cell adhesion on substrates or for detecting the neuronal markers expressed by the differentiated ADSCs. For visualizing the focal adhesions, control cells and cells stimulated with electric current were fixed in 4 % paraformaldehyde and permeabilized with 0.5% Triton X-100. Background binding was blocked with 3% bovine serum albumin (BSA) in PBS for 1 hour, followed by overnight incubation with mouse monoclonal anti-vinculin antibody (1:1000, from Sigma-Aldrich, Buchs, Switzerland) at 4 °C. After washing with PBS, samples were incubated in RT for 1 hour with Cy3-conjugated goat anti-mouse secondary antibody (1:100), DAPI (1:200) and phalloidin (1:500), all from Sigma-Aldrich.

Immunofluorescent staining was also used to visualize the neuronal markers expressed by the ADSCs subjected to current and/or copper stimulation in suspension. The cells were cultured on Lab-Tek 4-well chamber slides (Thermo Scientific, Nunc, Fisher Scientific AG, Wohlen, Switzerland) in growth medium for 4, 7, and 14 days after the stimulation. The cells were fixed in 4 % paraformaldehyde and permeabilized with 0.5% Triton X-100. The indirect immunostainings were performed at 4°C overnight. The neurogenic differentiation was confirmed using the neuron lineage-specific markers: mouse monoclonal anti-beta-tubulin isotype III (1:200, Sigma-Aldrich, Buchs, Switzerland) antibody and rabbit polyclonal anti-microtubule-associated protein 2 (anti-MAP-2; 1:00, Sigma-Aldrich) antibody. The slides were incubated with the appropriate secondary antibodies, Cy3-conjugated goat anti-mouse and anti-rabbit secondary antibody (1:1000, Sigma-Aldrich), in the dark at room temperature for 1 h. The slides were counter-stained with DAPI (1:200, 4',6-diamidino-2-phenylindole, Sigma) and phalloidin (1:200, Sigma-Aldrich). The slides were analyzed using a Leica fluorescence microscope (CTR 6000).

The number of cells expressing beta-tubulin isotype III or MAP-2 was determined by counting the DAPI stained cells and comparing this to the number of cells staining positive for the two markers in at least three microscopic fields per each chamber slide.

3.3.4.3 Real-time PCR

Real-time PCR was used to measure the mRNA expression levels of neuronal markers expressed by the ADSCs subjected to current and/or copper stimulation in suspension.

The total RNA was isolated using the SV Total RNA Isolation System kit (Promega, Dübendorf, Switzerland) according to the manufacturer's protocol, which included DNase digestion. The RNA was reverse transcribed with random primers (High-Capacity cDNA Reverse Transcription, Applied Biosystems). Pre-designed primers for rat Beta III-tubulin (HS00964962-g), MAP-2 (Hs01110346-m1), and eukaryotic 18S rRNA endogenous control (VIC®/MGB Probe, Primer Limited) were purchased from Applied Biosystems. The data were quantitatively normalized with the expression of 18S and were analyzed by measuring the threshold cycle (CT) values. For the quantification, the expression of each gene in the ADSCs was considered the 100% reference value. All of the values for mRNA expression were compared with the undifferentiated control.

3.3.4.4 Western blot

Western blot was used to measure the protein expression levels of neuronal markers expressed by the ADSCs subjected to current and/or copper stimulation in suspension. The cells were washed with cold PBS supplemented with a protease inhibitor cocktail (Sigma-Aldrich) and lysed with modified lysis buffer (50 mM Tris-HCl, pH 7.4, 150 mM NaCl, 10% glycerol, 1% Triton X-100 (Sigma-Aldrich), 2 mM EDTA, 10mM NapyroP, 200 uM Na3VO4, and 50 mM sodium fluoride). The protein lysate was measured using the BCA Protein Assay Kit (Thermo Scientific, Lausanne, Switzerland). 25 micrograms of the protein lysate of each sample was loaded on a 12% gel (Bio-Rad, Cressier, Switzerland). The separated proteins were electro-transferred onto a PVDF membrane (Immobilon-P; Millipore, Bedford, MA). The primary antibodies were anti-beta-tubulin isotype III (1:500)), and anti-MAP-2 (1:500). The membranes were washed and

incubated with the appropriate HRP-conjugated secondary antibody (Amersham Pharmacia Biotech, Dübendorf, Switzerland) in TBS with 0.1% Tween-20 and 5% non-fat dry milk for 1 h. The signals on the membranes were detected through the ECL method (ECL-Kit, Amersham Pharmacia Biotech, Germany).

3.3.4.5 Semiquantitative measurement of DNA

In addition to the impedance measurements, the ASC-seeded scaffolds were digested with papain (Sigma) at 60˚C overnight for quantification of DNA at 1, 2 and 3 weeks. A fluorometric assay based on the DNA-binding dye Hoechst 33258 (Bio-Rad, Hercules, CA) was used. The assay was performed according to manufacturer's protocol. The fluorescence was measured with a multilabel counter (Victor 3 1420, Perkin Elmer, Singapore).

3.3.6 Microscopy

All the bright-field and live/dead staining images were taken with Leica DM IL Microscope. The immunofluorescently stained cells were imaged with a Leica fluorescence microscope (CTR 6000). The cells within a scaffold were imaged with a confocal laser scanning microscope LSM 510 (Zeiss, Jena, Germany).

3.3.7 Statistical analysis

Non-parametric Spearman rank correlation was used to correlate the level of impedance in empty scaffolds. The plain PLA scaffold was correlated to each of the modified scaffolds either in control or chondrogenic differentiation media (n=3).

To determine the cell migration, adhesion and migration depth into the scaffold, three individual experiments were carried out in every current density group. Live and dead cells were counted on five different images taken from different locations of all scaffolds. All experiments were normalized to the number of cells entering the scaffold through the mesh without any applied current (100%). All the values are presented as mean ± SEM and one-way ANOVA was used to determine the statistically significant ($p<0.05$) differences between control and different current density groups.

For assessing cell spreading area and viability of cells adhered on substrates, three independent experiments were carried out in every current dose group described later. Cell spreading areas were determined and live and dead cells were counted at three different locations each, on both the current applied and control electrodes. For adhesion force measurements, force-distance curves of 43 cells in total were measured, each current dose group consisting of at least five measurements. Sensitivity of the cantilevers during the individual experiments has been calculated as the mean of three sensitivity measurements performed on different areas of the bare ITO substrate. Results are presented as mean ± SEM, and a non-parametric t-test with the Mann-Whitney test has been used to determine the statistically significant ($p < 0.05$, $p < 0.01$, and $p < 0.001$) differences between control and the different current dose groups.

For the stem cell differentiation studies, the data from cell proliferation, expression of beta-tubulin III and MAP-2 positive cells, and real-time PCR is presented as the mean ± SEM. In real-time PCR, two-way ANOVA was used to determine the statistically significant increase in expression in stimulated cells compared to the control. A p-value of $p<0.05$ was used to define statistical significance

All the statistical analyses were performed using GraphPad Prism 6 software.

4. Results

The results section presents how the electric stimulation affects the cell functions such as proliferation, viability, morphology, adhesion, and stem cell differentiation. In addition, the electrode materials used in the publications II-IV were characterized and their safe limits for applied electric currents and potentials are determined in the chapter 4.1. Chapter 4.2 presents how the cell proliferation characteristics change due to the applied electric stimulus and also how the cell number within a scaffold can be determined by the means of electric impedance. Results presented in the chapter 4.2 are from the publication I and II, and in addition to the proliferation of the cells

stimulated as suspension (publication II), the cells were stimulated as they were adhered on a substrate. In the chapter 4.3, the effect of current on cell morphology and viability, discussed in the publication II, and IV, is presented. Chapters 4.4 and 4.5 show how the electric stimulation affects the cell adhesion in two- and three dimensional environment (publications IV and III, respectively). Chapter 4.6 describes the different factors such as cell type and stimulation parameters that influence the cell response to the electric stimulation and chapter 4.7 shows that neuronal differentiation of adipose-derived stem cells can be triggered by using electric current and copper, phenomenon presented in the publication II.

4.1 Characterization of the electrode materials

This chapter presents the results of the electrode material characterization and the safe limits for the applied electric currents and potentials. Cyclic voltammetry (CV) was used to determine the electrochemical currents and potentials that result in oxidation and reduction processes at the electrodes used in the cell adhesion and neuron differentiation experiments. The characterized electrode materials were indium tin oxide (ITO), stainless steel and stainless steel coated with palladium, copper and platinum. From the CV, we obtained the current and potential limits for minimizing the damage to the electrode and generation of the reactive oxygen species (ROS) due to these processes. ITO electrodes were used in the publication IV and non-coated and coated stainless steel electrodes in the publications II and III.

The cyclic voltammogram of the ITO electrode showed that the oxidation begun at around 1.3 V (Fig. 12), thus using positive voltages until this limit prevents the damage to the electrode and the generation of redox species. In the further cell stimulation experiments, only positive currents were applied via the ITO electrodes.

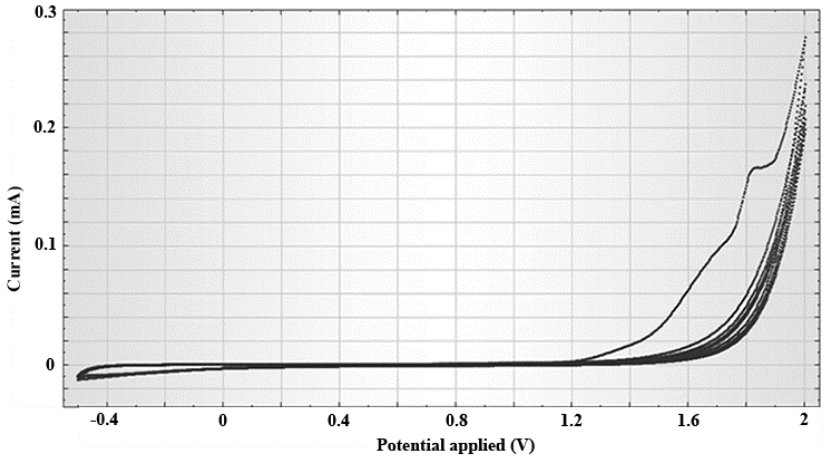

Figure 12. Cyclic voltammetry of ITO in cell culture medium.

In the adhesion into the scaffold and neuron differentiation experiments, stainless steel electrodes coated first a thin layer of palladium, then a thick layer of copper and last with a thin layer of platinum were used. The non-coated stainless electrode was stable in the voltage range of [-0.2, 1.2] V (Fig. 13 A) but due to the reshaping of the electrodes, stainless steel, palladium and copper parts were exposed to the electrolyte solution. The oxidation of the coated electrode took place also at very low positive potential values (Fig 13 B).

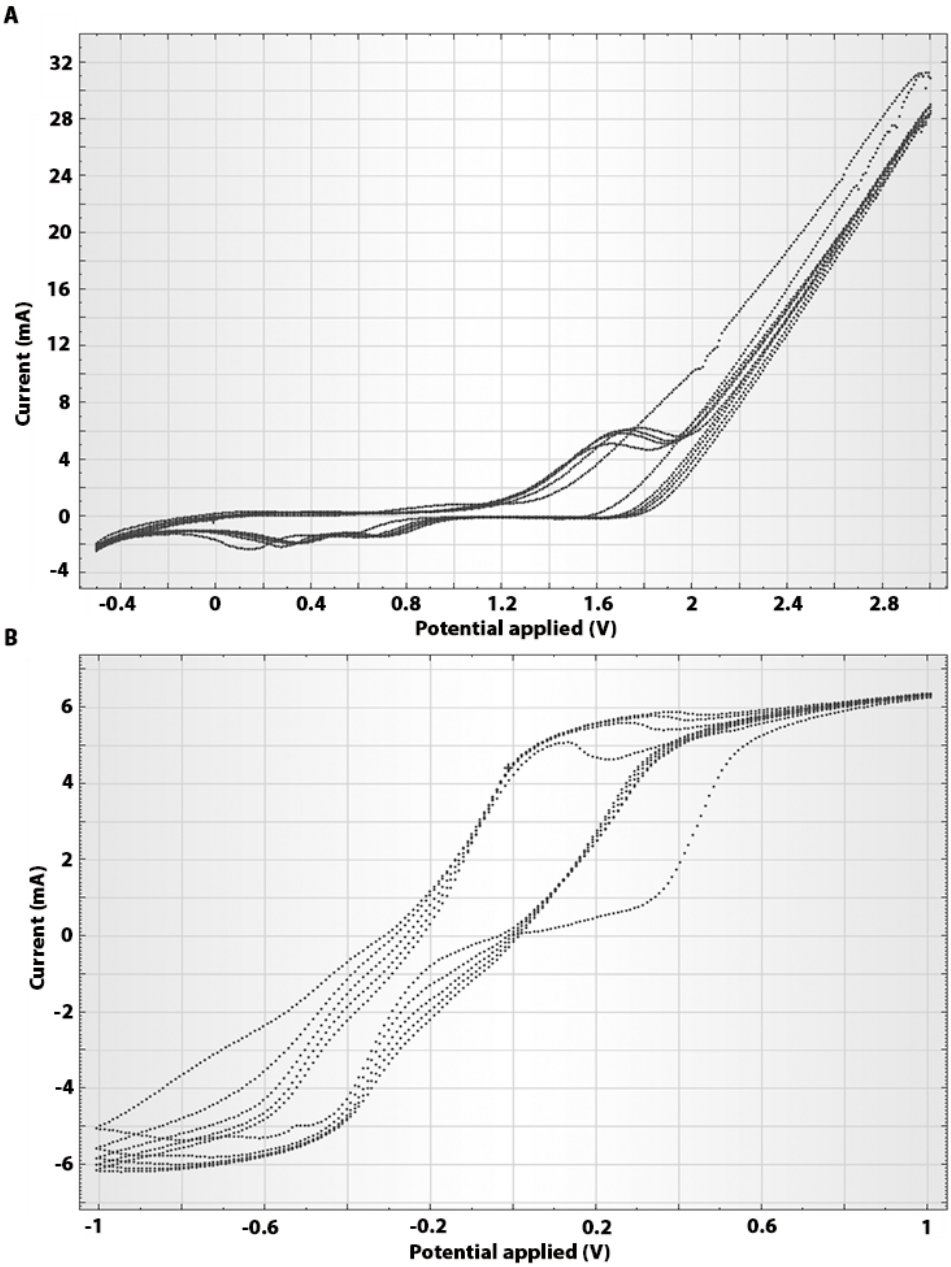

Figure 13. The cyclic voltammetry of non-coated stainless steel electrode (A) and the stainless steel electrode coated with palladium, copper and platinum (B).

As the applied currents had to be high enough to introduce changes to the cells, often the measured potential reached and exceeded the threshold for the redox reactions.

The maximum potential values measured when applying the highest current in each experimental condition are presented in the table 3.

Electrode material	Max. current density (A/m²)	Max. potential (V)
ITO	0.05	1.8
Pt	4	1.6
SS + Cu + Pd + Pt	6	0.6

Table 3. The electrode materials, the maximum current densities and the corresponding maximum potentials used in the viability, adhesion and differentiation experiments. The maximum current density value for the differentiation of adhered cells stimulated with copper and platinum electrodes was 3.6 A/m^2 but the potentials values are not available.

4.2. Cell number and proliferation

This chapter presents how the cell proliferation can be measured by the means of electric impedance and also how the electric stimulation and electrolysis affect the cell proliferation. The experiments were conducted with adipose-derived stem cells.

4.2.1 Measuring cell proliferation with electric impedance

In the publication 1, the correlation between the cell number within the scaffold and the measured impedance was studied. The measurements of the cell-seeded scaffolds at the day 1 showed that the more cells were seeded into the scaffolds, the higher the measured impedance was (Fig. 14). Cell proliferation in the scaffolds was demonstrated as a higher measured amount of DNA within the cells, corresponding to increase in cell number during culture. However, the time dependent correlation between the increase in cell number and expected increase in the impedance was not detected.

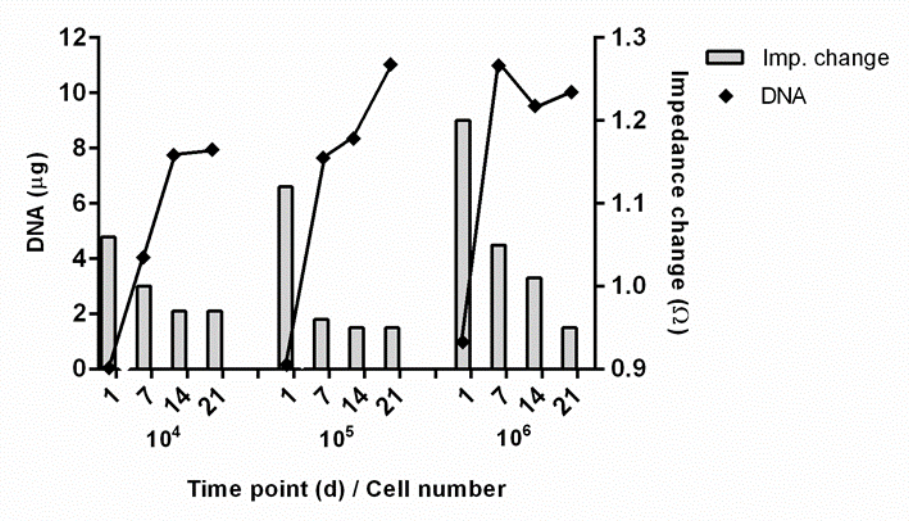

Figure 14. The changes in impedance and amount of DNA with respect to the seeded ADSC cell number in the PLA scaffold at 1, 7, 14, and 21 days of culture. Seeded cell numbers and time points are shown on the x-axis with respect to the measured impedance on the right y-axis, and amount of DNA on the left y-axis. DNA content reflects the cellularity in the scaffold. Impedance values of the scaffold with different cell numbers were derived by subtracting the impedance of the medium and the values were normalized to the impedance of the scaffold without cells at day 1. One scaffold of each initial cell seeding number (0, 10^4,10^5,10^6) was measured in every time point.

4.2.2 Effect of electric current (and copper electrolysis) on the cell proliferation

In addition to measuring the cell proliferation rates via electric impedance, we also studied how to influence the proliferation of ADSC with electric current and copper electrolysis. The ADSCs seeded on a glass slide and in suspension were subjected to electric current or additionally also to small amounts of Cu^{2+} released from the stimulating electrodes by electrolysis. The number of cells on day 4, 7, and 14 was counted and compared to the cell number at the day 4 control unless otherwise stated. The results of cells stimulated in suspension are presented in the publication II, and the results of cells adhered on a glass slide are presented only in this thesis.

When the stimulation with current only or current and copper was applied through platinum or copper electrodes to cells adhered on the glass slides, none of the stimulated cells showed as high proliferation rates as the control cells (Fig. 15 A). The cells exposed to both copper and current did not proliferate between days 4 and 7, however, at the day 14, the cell numbers were higher than at day 7. The increase in proliferation between days 7 and 14 was also observed when the cells were stimulated with current only. When the ADSCs were stimulated in suspension via platinum or copper coated stainless steel electrodes or with Cu^{2+} containing medium, the cells showed proliferation during the culture time in all the experimental groups (Fig. 15 B). The proliferation rates on control cells and cells stimulated with copper only were almost identical whereas the cells stimulated with current only proliferated much slower. Stimulation with copper + 1 mA increased the proliferation rate close to that of the control, and the highest proliferation rate was observed when stimulated with copper + 1.5 mA. The non-stimulated cells showed a similar proliferation rates both as adhered cells and cells in suspension, and the lowest cell numbers were counted when the cells were stimulated with current only. However, the clear decrease in proliferation between days 4 and 7 was only detected when stimulating the adhered cells.

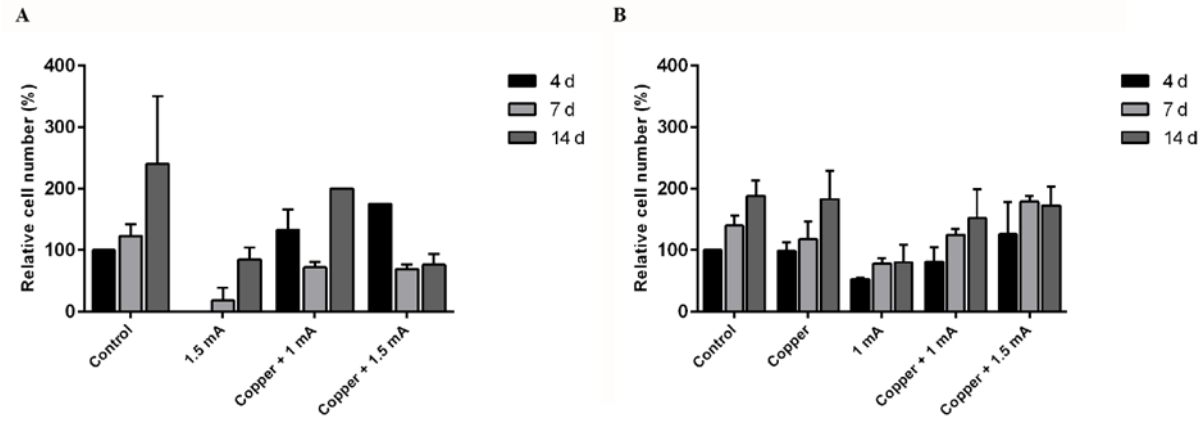

Figure 15. The proliferation of ADSCs adhered on a substrate (A) or in suspension (B) when stimulated with current or current and copper at the day 1. The cell numbers were compared to the 4 day control. The 4 day data for the adhered cells stimulated with 1.5 mA on a substrate was not available, thus the cell number from 1.5 mA

stimulation was compared to the 7 day control. The experiments were conducted with minimum of two different biological replicates and the cells were counted on at least three different locations on the substrate or the scaffold. The data represent the mean ± SEM.

4.3 Cell morphology and viability

This chapter presents the results of electric stimulation on cell morphology and viability. The effect of electric current on cell morphology and viability was studied after exposing the cells to different electric currents and most of the results are shown in this chapter are also presented in publications II and IV. The cell viability and morphology were analyzed in two different setups; the cells were either adhered on a substrate, either directly on the electrode (publication IV) or on a glass slide (not published data), or they were in suspension (publication II) while the stimulus was applied. Two different cell types were studied; mouse myoblasts (C2C12) adhered directly on the electrode, and human adipose-derived stem cells (ADSC) adhered on the glass slide or in a suspension. The cells were imaged with a bright-field microscope and for the morphology study, also stained using phalloidin and DAPI to visualize the cytoplasm and the nucleus, respectively. The viability was analyzed by staining the live and dead cells. In addition to the current, the ADSCs were also stimulated by small amounts of Cu^{2+} released from the electrodes via electrolysis and the viability was analyzed.

4.3.1 Morphology and viability of adhered cells

The viability and morphology of C2C12 cells adhered directly to the electrode or ADSCs adhered to the glass slide were analyzed after exposing the cells to an electric current. The current densities used here were 0.01 – 0.05 A/m^2 and exposure time 5 - 60 min.

The changes in morphology and viability of the C2C12s adhered directly on the ITO electrode is presented in the publication IV. Shortly, in the control conditions without an applied current the cells stayed spread on the electrode and showed very clear F-actin

fiber structures in the cytoplasm (Fig. 16 A). Small current doses below 14 As/m^2 applied to the adhered cells did not change the cell shape, (Fig 16 B), however, even with the small current densities, the cell area decreased compared to the control (Fig. 16 G). Current doses of 14 As/m^2 and higher caused the cells to shrink and become more round, and the cell size decreased even further. The F-actin fibers became less visible and the cells had started to lose the contact with the neighboring cells (Fig. 16 C-D). At current doses higher than 20 As/m^2, the cell shape had drastically changed, however some of the cells were still relatively spread when imaged with the bright-field microscope (Fig. 16 E), and there were cytoplasmic blebs observed. The cytoskeleton of the phalloidin-stained cells looked distorted and showed no longer visible F-actin fibers (Fig. 16 E). The cells on the electrode at different current doses were stained for live and dead cells and the number of live and dead cells was counted and presented as a percentage of the total number of the cells on the electrode (Fig. 16 F). There was always approximately 1 % of dead cells on the electrode and the current doses up to 11 As/m^2 did not increase the number of the dead cells. At higher doses the cell viability started to decrease and was 60 ± 15 % at the doses of 11-16 As/m^2 and 37 ± 16 % at doses above 16 As/m^2. Nearly all the cells were dead with current doses higher than 20 As/m^2.

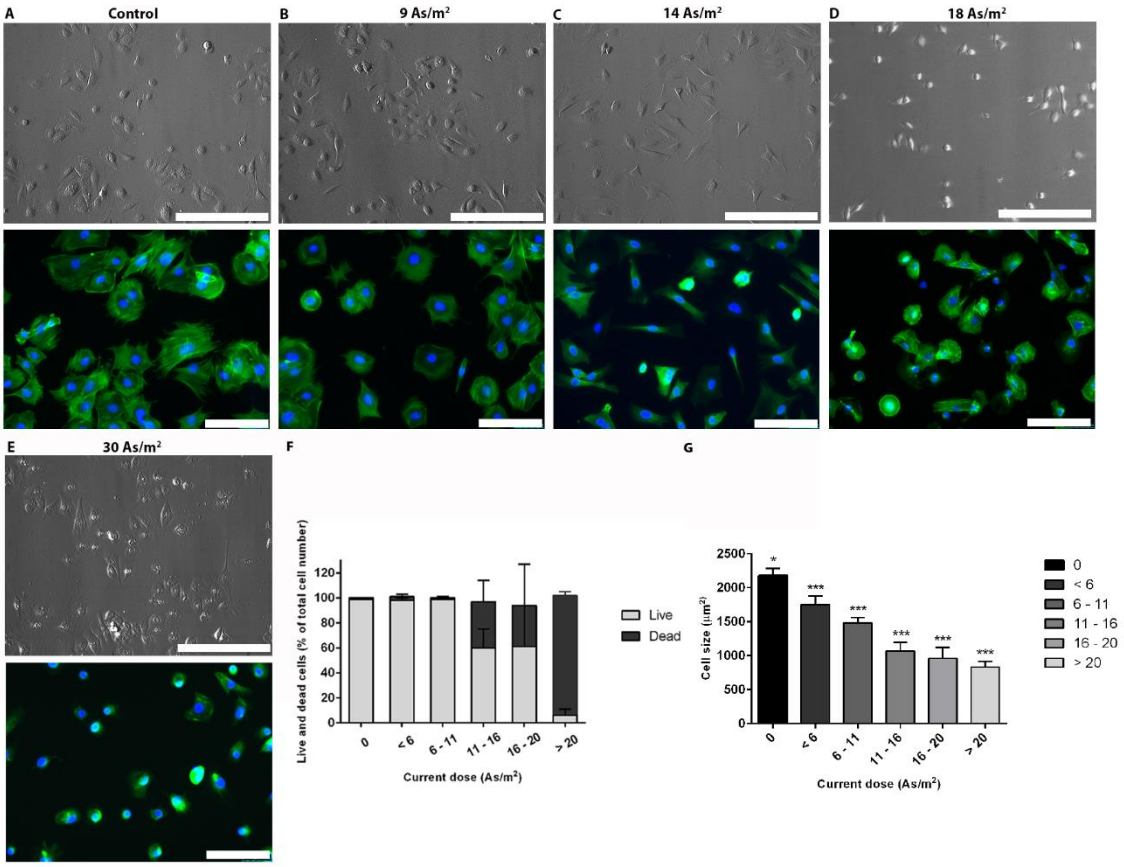

Figure 16. Bright-field and fluorescent images of C2C12 cells adhered directly on the electrode in control conditions (A) and exposed to different current doses (B-E). The cells in the fluorescent images were stained with phalloidin for the F-actin in the cytoplasm (green), and with DAPI for the nucleus (blue). Scale bars in the bright-field images are 100 µm and in the fluorescent images 25 µm. The number of live and dead C2C12 cells (F) and the cell spreading area at different current doses. Data are presented as mean ± the standard error, while single and triple asterisks indicate $\rho < 0.05$ and $\rho < 0.001$ significance levels as compared to the control, respectively. The number of repetitions for control, <6, 6-11, 11-16, 16-20, and >20 As/m^2 was *n=7, n=3, n=3, n=6, n=2, and n=3*, respectively. Data are presented as mean ± SEM.

Figure 16 F presents the cell viability one hour after the current simulation was ended. However, at current doses higher than 11 As/m^2, even the cells that stained alive one hour after the exposure to the current, failed to stay alive until the next day (non-

published data). Figure 17 shows the bright-field images of the cells on the electrode (inside the black rectangle) and control 24 – 72 hours after the current exposure. Only at the current dose of 11 As/m^2 or lower, the cells were alive also on the current electrode. Higher current dose exposure resulted in the death of all the cells on the electrode. However, the cells on the control stayed alive and were to some extent able to migrate and adhere to the electrode.

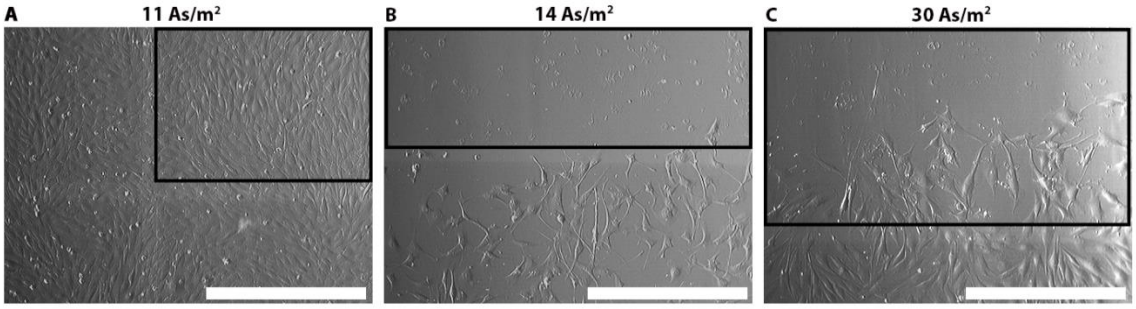

Figure 17. C2C12 cells on the electrode (black rectangle) and control imaged 24 -72 hours after the 1 hour exposure to current doses of 11 As/m^2 (A), 14 As/m^2 (B), and 30 As/m^2 (C). Scale bars are 100 µm.

When the ADSC cells were adhered on a glass slide and the current was applied through the copper electrodes placed on both sides of the slide but without a direct contact to the cells, the viability was affected only with relatively high current densities and doses (non-published data). The viability was studied 72 hours post-stimulation when the cells were exposed for one hour to the currents of 1.5, 10, and 20 mA that result in current densities of 3.4, 28, and 48 A/m^2 and current doses of 2.6, 17 and 34 mAs/m^2, respectively. At current of 1.5 mA there was no decrease in cell viability compared to the control whereas in average 50% of cells stained dead after exposed to 10 mA. At the current of 20 mA, there were no live cells detected. The distance of the cells from the stimulation electrodes had an influence on the cell viability; the closer the cells were to the working electrode where the Cu^{2+} was released to the culture medium, the more dead cells were detected.

The morphological changes of ADSC cultured on a glass slide and stimulated with 1 mA and copper at day 1 were analyzed at day 4, 7, and 14 (Fig. 18). The non-

stimulated ADSCs maintained their adipose-like flat shape whereas the stimulated cells appeared more elongated even at day 14 after the stimulation. The current of 1 mA for one hour equals to a current density of 2.4 A/m^2 and current dose of 1700 As/m^2.

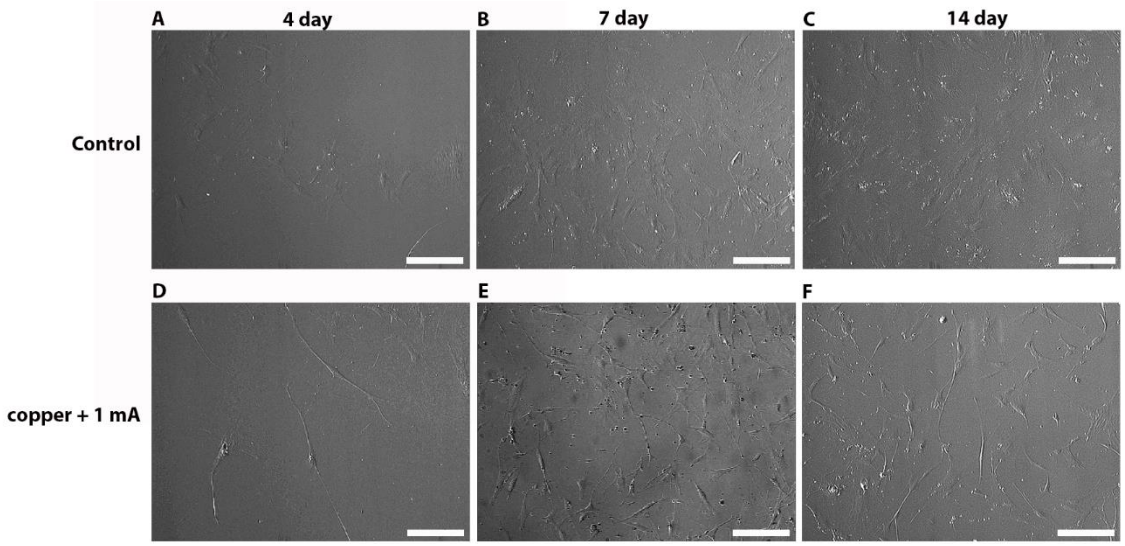

Figure 18. The ADSCs in the control conditions (A-C) and stimulated with a current of 1 mA (D-F) at days 4, 7, and 14. Scale bars are 100 µm.

4.3.2 Morphology and viability of cells stimulated as suspension

In addition to the adhered cells, the viability and morphology was studied after the ADSCs were exposed to current in suspension and later seeded on the culture plates for the analysis. The cells were stimulated for 1 hour with a monophasic pulsed current (5 s on, 20 s off) with the current of 1 mA and 1.5 mA that result in a current density of approximately 4 A/m^2 and 6 A/m^2 and current doses of 2900 and 4350 As/m^2. The results are presented in the publication IV.

Shortly, due to the stimulation of ADSCs in suspension, the cell viability reduced to 78 ± 11 %, measured right before and immediately after the 1 h stimulation and before seeding the cells to the culture plates. There was no significant difference in the cell viability between the different stimulation conditions. The viability was not studied with live/dead staining in the later time points, however all the cells stained for nucleus and cytoplasm at time points of 4, 7, and 14 days appeared live.

The stimulation of ADSCs in suspension changed the morphology when the cells were exposed to an electric current both with and without the copper (Fig. 19). The cells showed a significant elongation compared to control cells and cells stimulated with copper alone that maintained their adipose-like, spindle-shaped morphology. The elongation was observed as a reduction of cytoplasm to nucleus ratio. The morphological changes were observed already at day 4 and they were maintained throughout the observation time of 14 days.

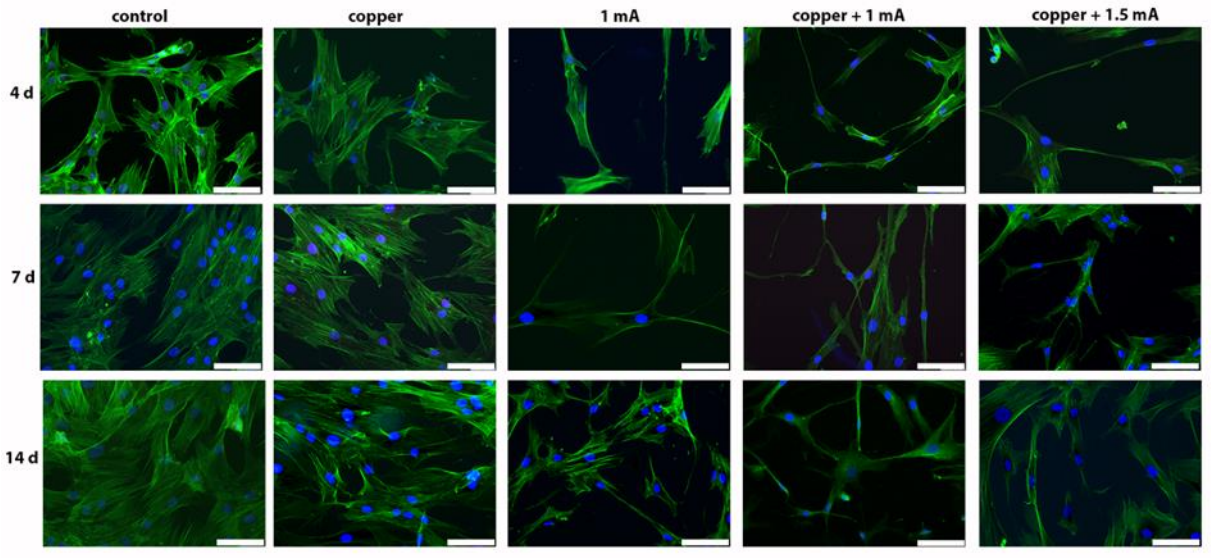

Figure 19. The changes in the cell morphology when the ADSCs in suspension were stimulated with copper, current or both. The cell cytoplasm was stained with phalloidin (green) and nucleus with DAPI (blue). Scale bars are 100 µm.

4.4 Cell adhesion on two-dimensional substrates

This chapter presents how the electric stimulation affects the cell adhesion on two-dimensional substrates. The C2C12 cell detachment from the substrate due to an applied electric current was studied with two methods; a qualitative washing assay where the possible weakly adhered cells were rinsed away from the substrate and the remaining cells were counted, or with the FluidFM that allowed the direct quantification

of the cell-substrate adhesion forces. The cells were in a direct contact with the electrode and exposed to current densities of 0.01 – 0.03 A/m^2 for 1 - 60 min. Current doses (As/m^2) were calculated from the total current on time for each current density. The data presented in this chapter can be found in the publication IV.

The data obtained from the washing assay showed that the total number of cells, including both live and dead cells, on the electrode was higher compared to the control at current doses up to 11 As/m^2 (Fig. 20 A). At current doses higher than that, the total number of cells on the current electrode was slightly smaller compared to the control, however none of these changes were significant. On average, at current doses higher than 11 As/m^2 it was possible to rinse off approximately 25 % of the cells.

When only the number of the live cells on the electrode was considered, there were significantly less viable cells on the electrode with the current doses above 11 As/m^2 compared to the control (Fig. 20 B).

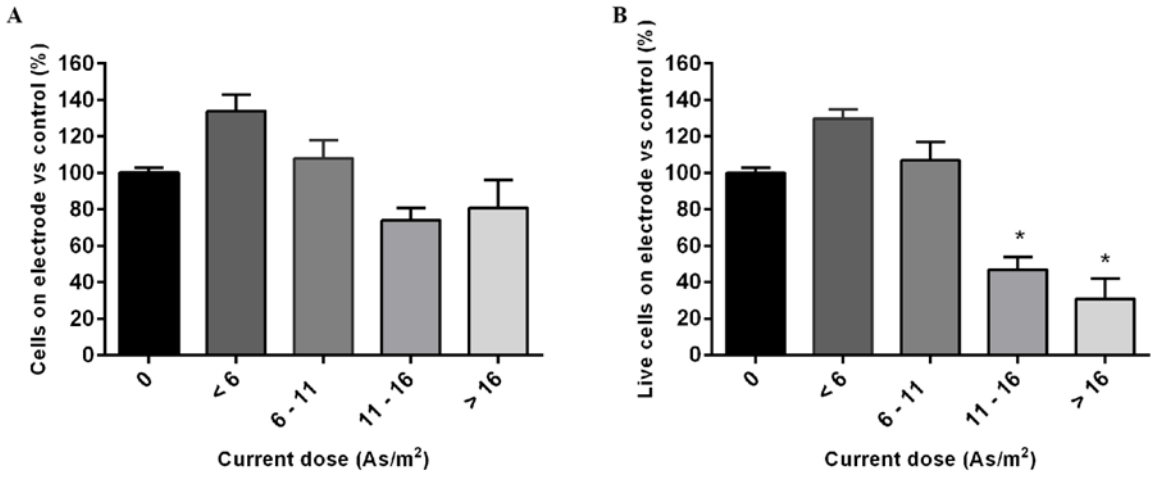

Figure 20. The total number of C2C12 cells (A) and the number of live cells (B) on the electrode compared to the control. The number of repetitions for control, <6, 6-11, 11-16, 16-20, and >20 As/m^2 was *n=7, n=3, n=3, n=6, n=2, and n=3*, respectively. Data are presented as mean ± SEM, asterisk indicating $\rho < 0.05$ significance level.

According to the washing assay, there was no decrease in the adhesion of the cell population to the substrate at current doses below 11 As/m^2 but at higher current

doses, a portion of the cells could be rinsed off of the electrode. To study how this translated to the actual cell adhesion forces, we quantified the forces with the FluidFM. Figure 21 presents the top view of the pickup process.

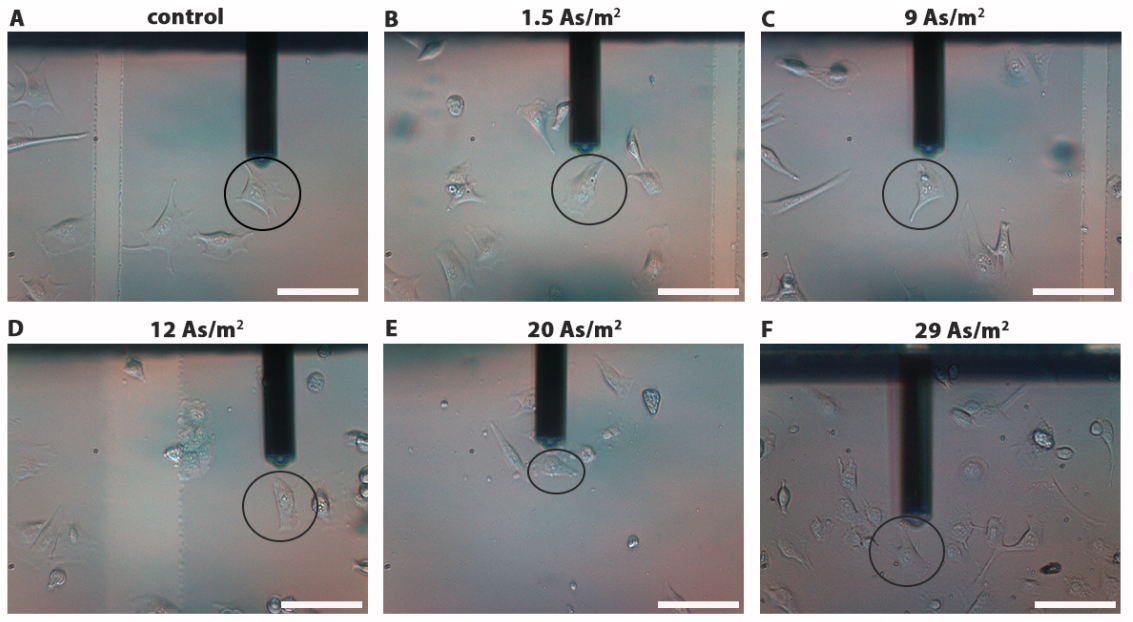

Figure 21. Top view of the pickup process. The image was taken before the cell adhesion measurement, the circle indicates the C2C12 cell targeted by the FluidFM cantilever. Scale bars are 100 µm.

Force-distance curves of single-cell detachment were recorded with the FluidFM and the corresponding curves in control conditions and after the current exposure are presented in figure 22. The force-distance curves depict the characteristic properties of the cell adhesion, including the maximum cell adhesion force (detachment force), detachment distance and the total work needed to detach the cell (detachment work).

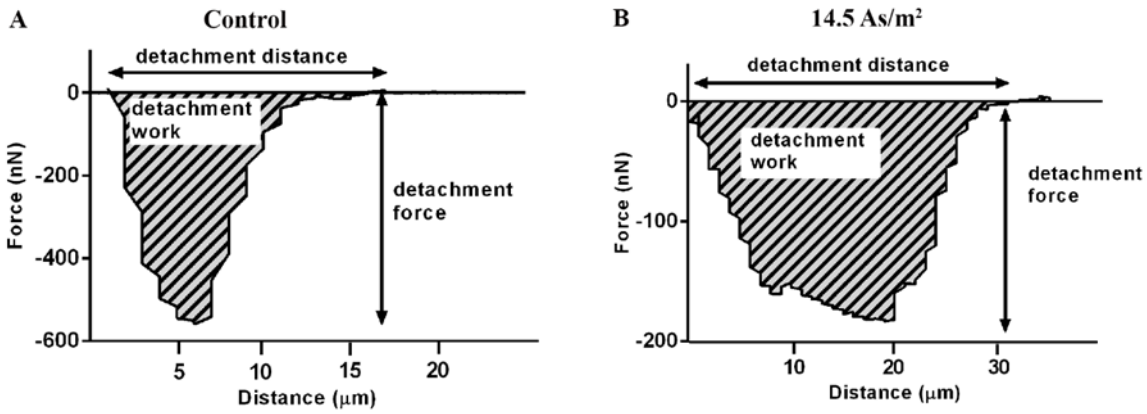

Figure 22. Representative examples of the force-distance curves in control conditions and after the C2C12 exposure to current dose of 14.5 As/m^2. Detachment force is determined as the maximum force needed to detach the cell from the substrate, detachment distance is the vertical distance the cantilever was retracted before the cell was completely retracted and the detachment work was calculated as the integral of the force-distance curve.

The cell adhesion in control conditions was measured with two different FluidFM setups; a commercial setup from Cytosurge and a custom-build setup called Skeleton. Cell adhesion to the substrate (ITO) measured with the two setups showed very little, non-significant setup-dependent variations. The maximum cell adhesion force was 516 ± 70 nN and 550 ± 103 nN, detachment distance 23.4 ± 1.4 µm and 24.7 ± 4.7 µm and total detachment work 6.6 ± 0.9 pJ and 5.4 ± 1.2 pJ for the Cytosurge and Skeleton setups, respectively (Fig. 23)

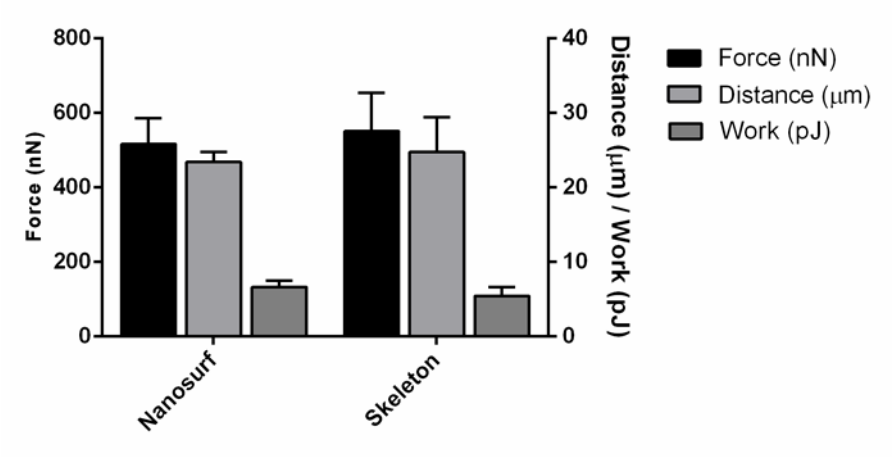

Figure 23. The maximum adhesion force, detachment distance and total detachment work of C2C12 cells on the ITO substrate without an applied current. For data measured with Nanosurf, *n=22*, and with Skeleton, *n=10*. Data are presented as mean ± SEM.

The cell adhesion under the electric current was quantified with the commercial Cytosurge setup. As observed in the washing assay, there were no changes in the cell adhesion at current doses below 11 As/m^2. This was in agreement with the adhesion force measurements that showed no decrease in cell detachment forces compared to the control (Fig 24). At current doses of 11-16 As/m^2 it was possible to detach about 25 % of the cells. This increase in the detachment rate in the whole cell population correlated with the measured single-cell adhesion forces; the detachment force in the control conditions was 516 ± 70 nN whereas exposing the cells to current doses of 11-16 As/m^2 resulted in detachment forces of 288 ± 30 nN. At current doses higher than 16 As/m^2, the detachment force was significantly higher than that in the control conditions while according to the washing assay, these current doses resulted in a smaller number of cells adhered to the substrate compared to the control. The detachment distance, i.e. the distance that the cantilever was be retracted from the surface to detach the cell completely, increased already at the current doses above 6 As/m^2 and at current doses above 11 As/m^2, the distance was significantly higher compared to the control, sometimes even exceeding the maximum cantilever retraction length possible with the commercial setup. Similar to the detachment distance, also the

total work needed to detach the cell was first increasing compared to the control but then, like the detachment force, dropped at the current doses of 11-16 As/m^2.

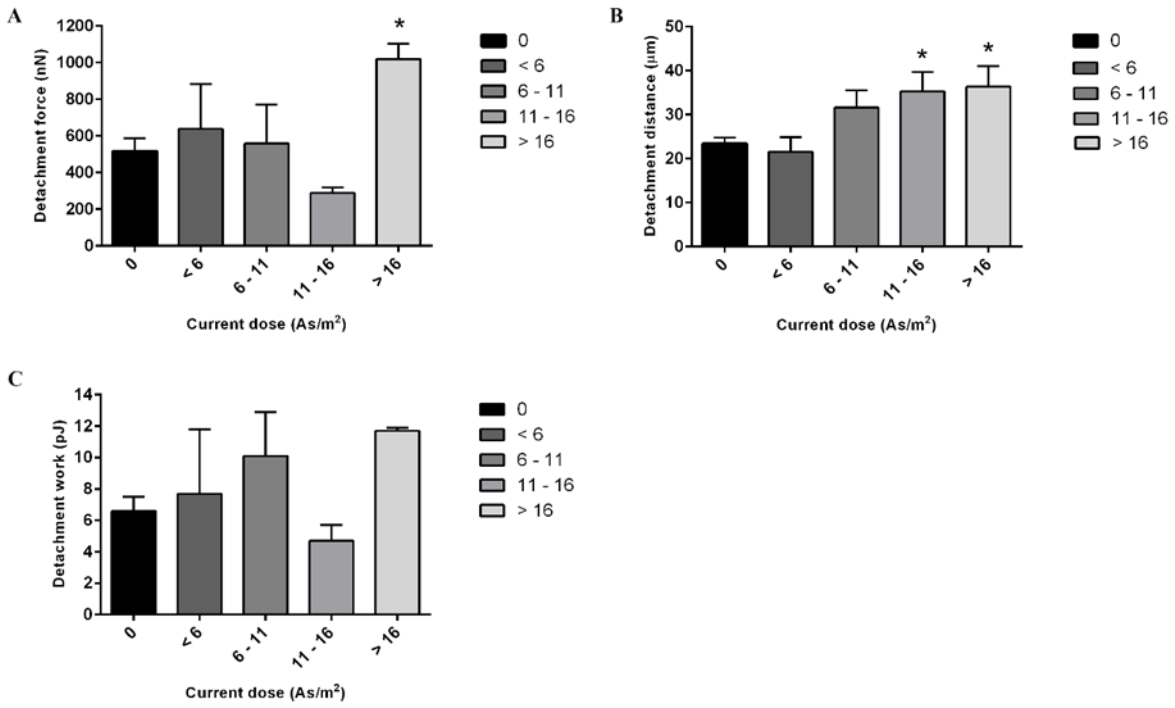

Figure 24. Detachment force (A), detachment distance (B), and detachment work (C) of C2C12 cells at different current doses. Each current dose group consists of at least five independent measurements. Data are presented as mean ± SEM, asterisk indicating $\rho < 0.05$ significance level as compared to the control.

Cells adhere to the substrate through the focal adhesion points where vinculin is one of the most prominent part of the adhesion complex. In order to find out if stimulation with electric current caused changes in the focal adhesion sites, cells were stained using vinculin and additionally using phalloidin and DAPI to visualize the cells (Fig. 25)

In control conditions and in current doses up to 9 As/m^2, vinculin was aggregated into focal adhesions at the ends of the actin fibers stained by phalloidin (Fig. 25 a-c). At the higher current doses vinculin structures became less visible (Fig. 25 d-e) and at current doses of 18 As/m^2 the vinculin structures had disassembled (Fig. 25 f).

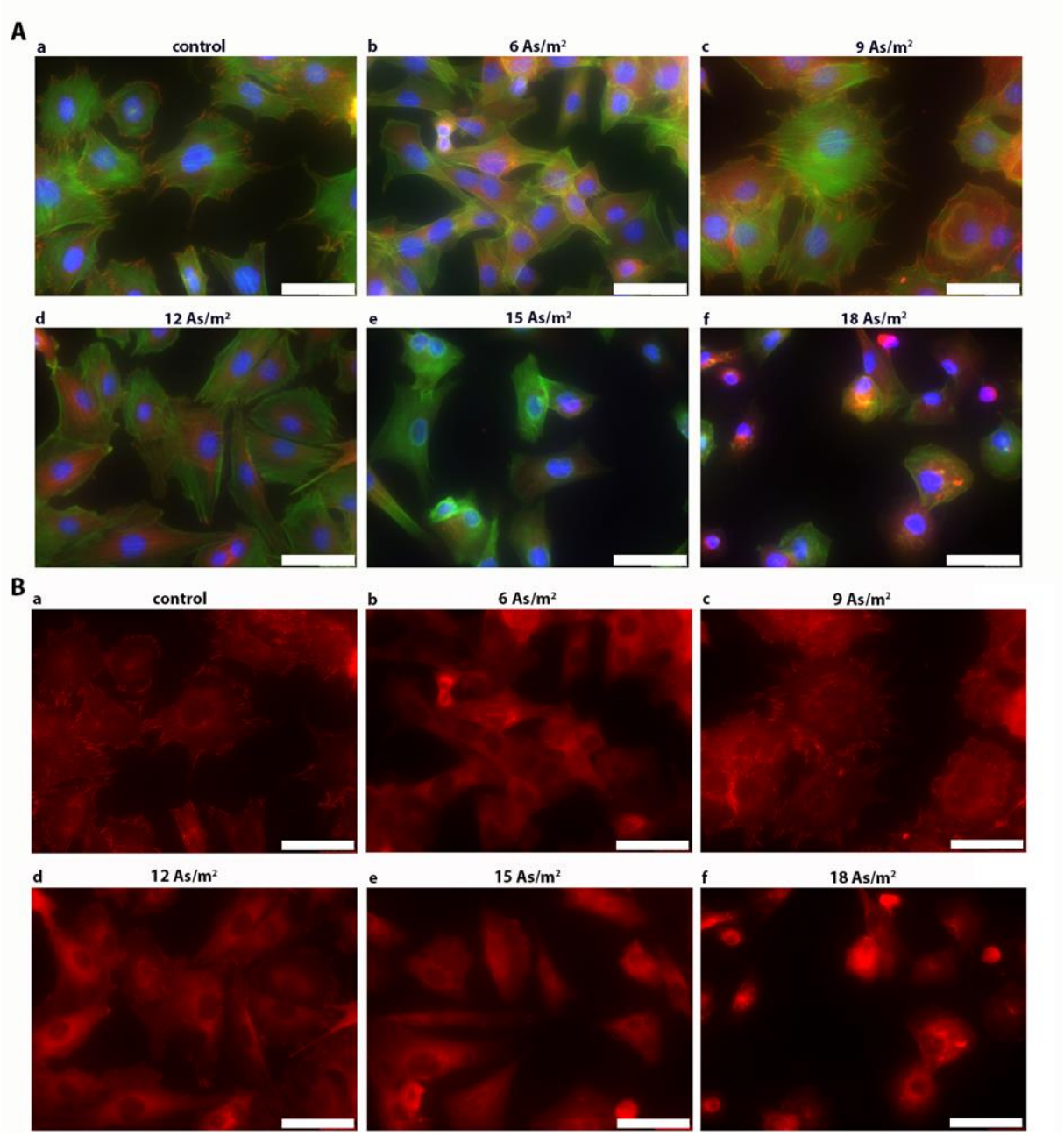

Figure 25. Fluorescent images of C2C12 cells in control conditions (a) and as stimulated at different current doses (b-f), stained with vinculin (red), phalloidin (green) and DAPI (blue) (A) and the vinculin stained focal adhesion sites presented alone (B). Scale bars are 50 µm.

4.5 Cell adhesion and migration in three-dimensional constructs

This chapter presents how the C2C12 cell migration and adhesion into a biomaterial scaffold change due to an applied electric current (publication III). A non-conductive scaffold was surrounded with conductive metal meshes and when no current was applied to the meshes, the cells were able to adhere to the meshes and further migrate through the pores to the scaffold and adhere to it. Mesh pore size played an important role in the cell migration to the scaffold. If the mesh pore size was more than 60% smaller than the cell size, the cells were not physically able to migrate through the mesh to the scaffold. If the mesh pore size was much bigger than the cell size, the cells were able to migrate into the scaffold despite the applied current. The used mesh pore size was approximately 90% of the average cell size, measured prior to each experiment. C2C12 cultures had a very homogeneous cell distribution and the number of cells that were bigger or smaller than the average size was almost negligible.

When a current of 0.3, 1, or 1.5 mA, that result in current densities of approximately 1, 4, and 6 A/m^2 and current doses of 720, 2900 and 4350 As/m^2, respectively, was applied to the mesh, the number of the cells attached to the mesh and into the scaffold and also the cell migration depth into the scaffold decreased (Fig. 26). At the current of 0.3 mA (Fig 26 B) very few C2C12 cells attached to the mesh anymore and also the cell number in the scaffold after one hour was significantly lower compared to the control experiment (Fig. 26 E). With higher currents of 1 mA and 1.5 mA (Fig. 26 C-D), no cells attached to the mesh and the number of C2C12 inside the scaffold decreased further. All cells that adhered to the scaffold were alive; no dead cells were detected. Cell migration depth into the scaffold was also related to the applied current (Fig. 26 F). In control conditions, with no current applied to the mesh surrounding the scaffold, cells migrated approximately 390 µm inside the scaffold. With a current, cell migration depth into the inner parts of the scaffold decreased, however the differences are not statistically significant.

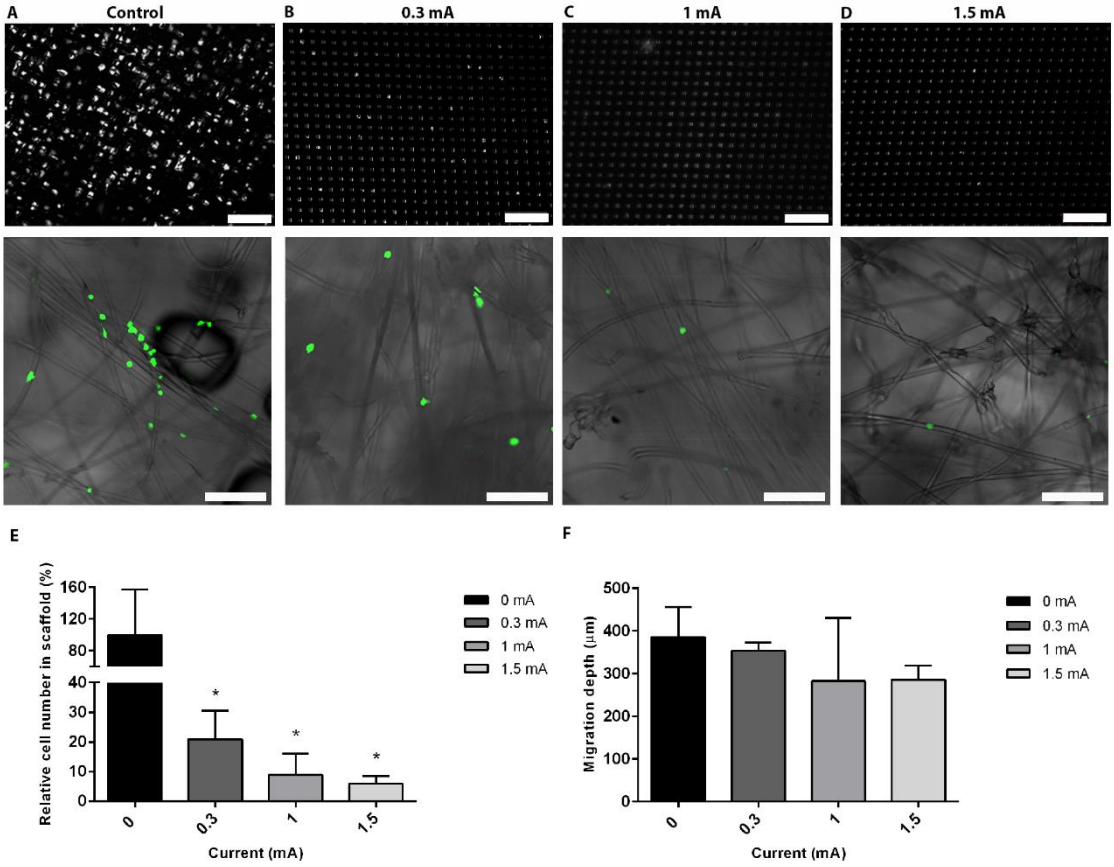

Figure 26. C2C12s on the electrode and in the scaffold in control condition (A) and with different currents (B-D). Cells adhered to the electrode are seen as white dots and cells adhered into the scaffold as green dots Scale bars are 200 µm. C2C12 number in the scaffold, normalized to the control condition (E) and the cell migration depth inside the scaffold (F) due to the increase in current. The data represent the mean ± SEM of triplicates; the asterisk indicates $p < 0.05$ with respect to the control.

4.6. Factors influencing the cell response to the electric stimulation

4.6.1 Effect of the cell type

While many of the cell mechanical properties are cell-type dependent, we performed the washing assay to determine if this applies also to the cell adhesion under the applied electric current. For this, we applied a current density of 0.5 A/m^2 or 1 A/m^2 that correspond to the current of 0.65 and 1.3 mA and current dose of 360 and 720 As/m^2, respectively, to the electrode and seeded either C2C12s or ADSCs on it. The number of live and dead cells adhered on the electrode was counted in relation to the current density after one hour of current exposure.

All the cells that were able to adhere to the electrode despite the current, were alive. However, there were significant differences between the number of the adhered cells; with both current densities, there were nearly three-fold of C2C12 than ADSC adhesion on the electrode (Fig. 27).

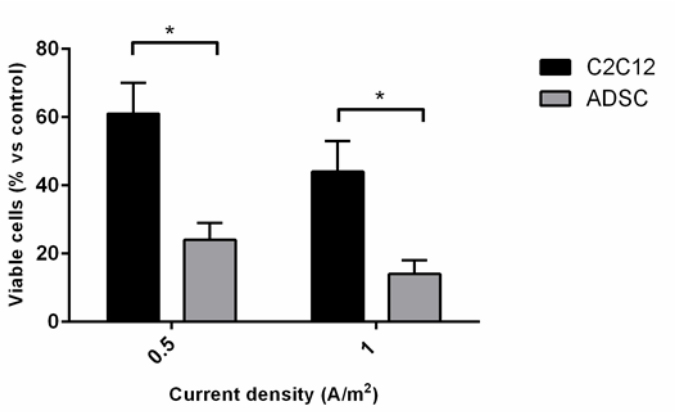

Fig 27. The percentage of the C2C12 cells and ADSCs adhered to the electrode with an applied current of 0.5 A/m^2 and 1 A/m^2 compared to the control without the current. Data are presented as mean ± the standard error, asterisk indicating $\rho < 0.05$ significance level.

4.6.2. Effect of stimulation conditions and parameters

The cells were stimulated in several different conditions and with different electrode configurations; the cells were either adhered directly on the electrode, they were seeded on a glass slide without a direct contact to the electrodes, or they were in suspension. In addition, the electrode materials were different in different setups. Table 4 presents the different stimulation conditions and electrode materials as well as the maximum limits for current, current density and current dose used for stimulating the two different cell types used in this thesis.

The cells directly adhered to the electrode were the most susceptible to the current; already currents as small as 5 µA had an effect on the cell viability. When the cells were adhered on a glass slide without a direct contact to the stimulating electrodes, or in a suspension, the cells were able to withstand the currents around 1.5 mA without showing changes in the viability.

Electrode	Condition	Cell type	Current (µA)	Current density (A/m^2)	Current dose (As/m^2)	Publication
ITO	Adhered on electrode	C2C12	5	0.05	14	IV
Cu, Pt	Adhered on glass slide	ADSC	1500	3.4	2600	-
SS+Cu+Pt, Pt	In suspension	ADSC	1500	6	4350	II, III

Table 4. The different stimulation conditions and the limits for the current, current density and current doses used in the stimulation of the cells, and the corresponding publications. The stimulation of the cells adhered on the glass slide is non-published data.

Generally, the cell viability and adhesion/detachment are presented in relation to the current dose when the cells were seeded on the electrode and thus in a direct contact with it. Up to the current dose of 18 As/m^2, there was no changes in the viability, determined as a number of live cells on the electrode compared to the total number of cells on the electrode, due to an increase of current density from 0.01 A/m^2 to 0.03 A/m^2 (Fig. 28). Also the number of adhered cells on the electrode compared to the control at current doses below 16 As/m^2 seemed to be dependent only on the dose but with current doses above that, also the current density and the exposure time played a

role. When cells were exposed to the current dose of 18 As/m^2, the number of cells adhered to the electrode decreased more with a current density of 0.01 A/m^2 applied for 60 min than 0.03 A/m^2 applied for 20 min.

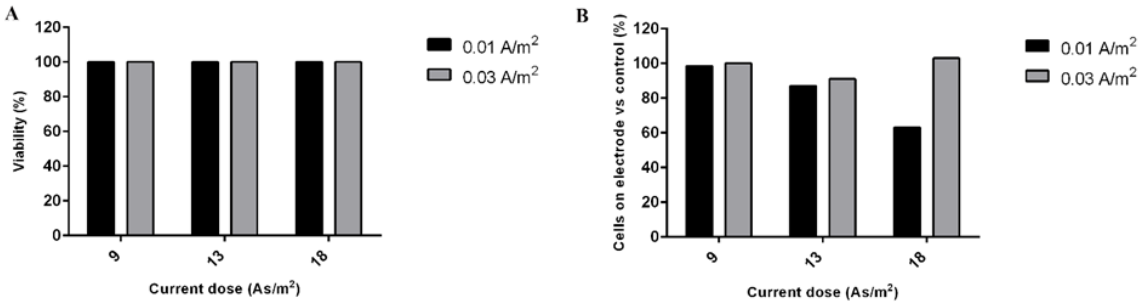

Figure 28. The percentage of live C2C12 cells (A) and C2C12 cells adhered on the electrode (B) compared to the control in relation to the applied current density and dose. Values from single measurements are presented.

Several ITO electrodes were used in the experiments and while the ITO resistance showed small electrode-to-electrode variations, the potential difference between the working and counter electrode was adjusted by the potentiostat in order to keep the current constant. The potential generally stayed within the safe limits, [-0.5, 1.7] V that did not cause damage to the electrode. However, even in the higher potential values, there was no effect on the cell viability as long as the applied current doses were below the lethal limit of around 14 As/m^2 (Fig.29). For instance, 9 As/m^2 with a potential of 1.8 V did not decrease the cell viability, whereas 15 As/m^2 with a potential of 1.1 V resulted in a cell viability of only 19 %.

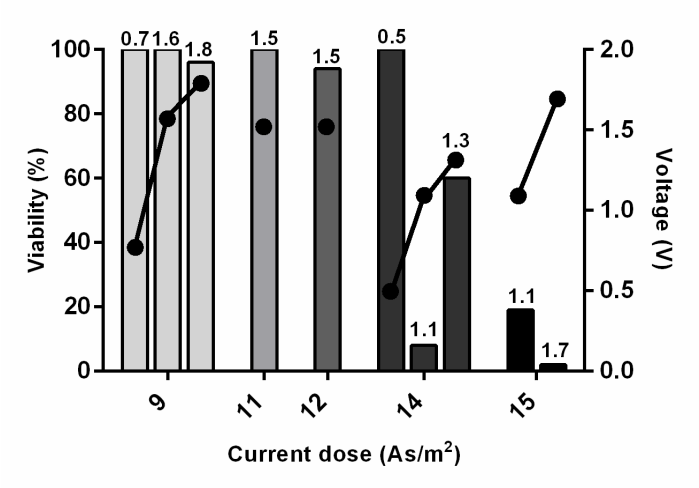

Figure 29. The C2C12 cell viability on the electrode in relation to the current dose and potential. The viability is shown in the left y-axis as a bar plot and voltage in the right y-axis as a line chart. Even the high potential values (i.e. 1.8 V) did not decrease the cell viability as long as the applied current doses were below the lethal limit of around 14 As/m^2. Values from single measurements are presented.

4.6.4. Experiment-to-experiment variation

Although the cell viability and adhesion was in general correlated with the current dose, there was also experiment-to-experiment variation. In spite of identical current, stimulation time and potential within two different experiments, we still occasionally observed differences in the viability and adhesion properties. A current dose of 12 As/m^2 for 10 min with a voltage of 1.5 V, resulted in 90 % and 98 % viability and 52 % and 98 % total adhesion in two separate experiments. The cell passage number was P35 and P9, respectively.

4.7 Neuronal differentiation with electric current and copper

In this work, we investigated the effect of electric current and/or copper on neuronal differentiation of adipose-derived stem cells. Two different experimental setups were used; the cells were either adhered on a substrate or they were in suspension during

the stimulation. In either setup, the cells had no direct contact to the electrodes, and the stimulation setup of cells in suspension was the same as described in the chapter 5.5. Cells from both experimental setups were analyzed post-stimulation for the protein expression with immunohistochemical staining. In addition, the cells stimulated in suspension were analyzed with western blotting and also for the mRNA expression with RT-PCR. The results of cells stimulated as a suspension are presented in the publication II, and the results of stimulation of adhered cells is non-published data.

4.7.1 Immunohistochemistry

The expression of beta-tubulin isotype III, a marker for immature neurons, was studied at 4, 7, and 14 days after stimulation of cells in suspension and at 7, and 14 days after stimulation of adhered cells.

When studied the cells stimulated in suspension positive expression of the beta-tubulin isotype III, a marker for immature neurons, was observed already at day 4 when the ADSCs were stimulated with copper with or without current, but the expression levels were clearly highest with the current of 1.5 mA and the Cu^{2+} gradually released to the cells via electrolysis (Cu + 1.5 mA). (Fig. 30) At day 7, the expression levels stayed approximately the same or decreased slightly. Cells stimulated with current alone remained negative at day 4 and 7. At day 14, only the ADSCs stimulated with both copper and current of 1 mA showed a further increase in expression of beta-tubulin isotype III whereas the expression in cells stimulated with copper alone or Cu + 1.5 mA decreased. Interestingly, a positive expression of cells stimulated with current only appeared only at day 14. There was no expression in control cells in any time point. The highest expression of beta-tubulin isotype III was observed at day 7 when cells were stimulated with Cu + 1.5 mA.

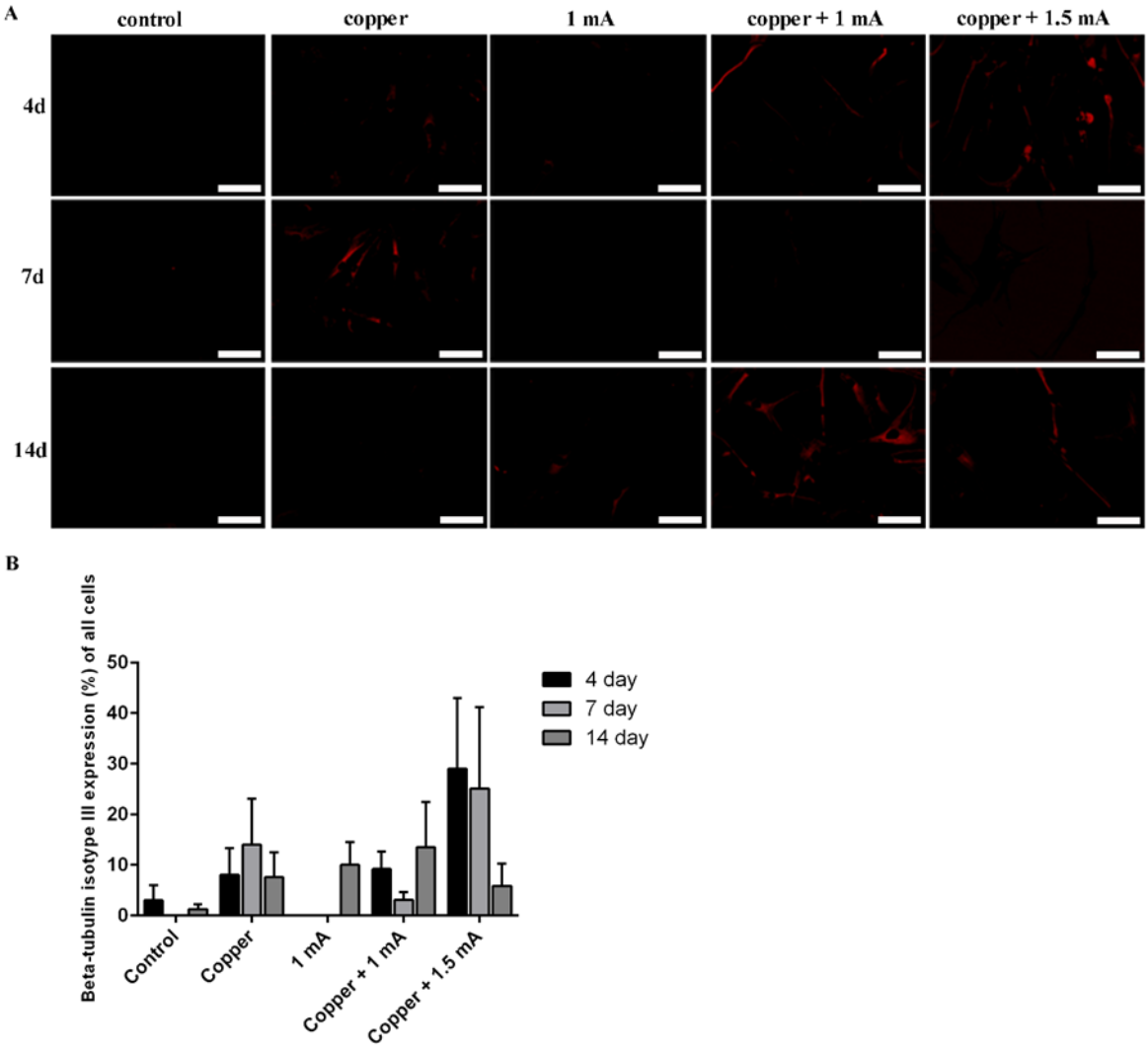

Figure 30. Fluorescent images (A) and graphs presenting the percentage of positive ADSC stained with anti-beta-tubulin isotype III neuronal antibody (B) at 4, 7, and 14 days when the cells were stimulated in suspension. Scale bars are 100 µm. The data in graphs represent the mean ± SEM of triplicates.

The highest expression of beta-tubulin isotype III was observed after the stimulation with both copper and current also when the cells were adhered on the substrate (Fig. 31). The stimulation with copper only resulted in no expression whereas the stimulation with current only (1.5 mA) increased the expression to the similar level than the

stimulation with Cu+ 1.5 mA. As with the cells stimulated in suspension, the highest expression of beta-tubulin isotype III was detected at day 7.

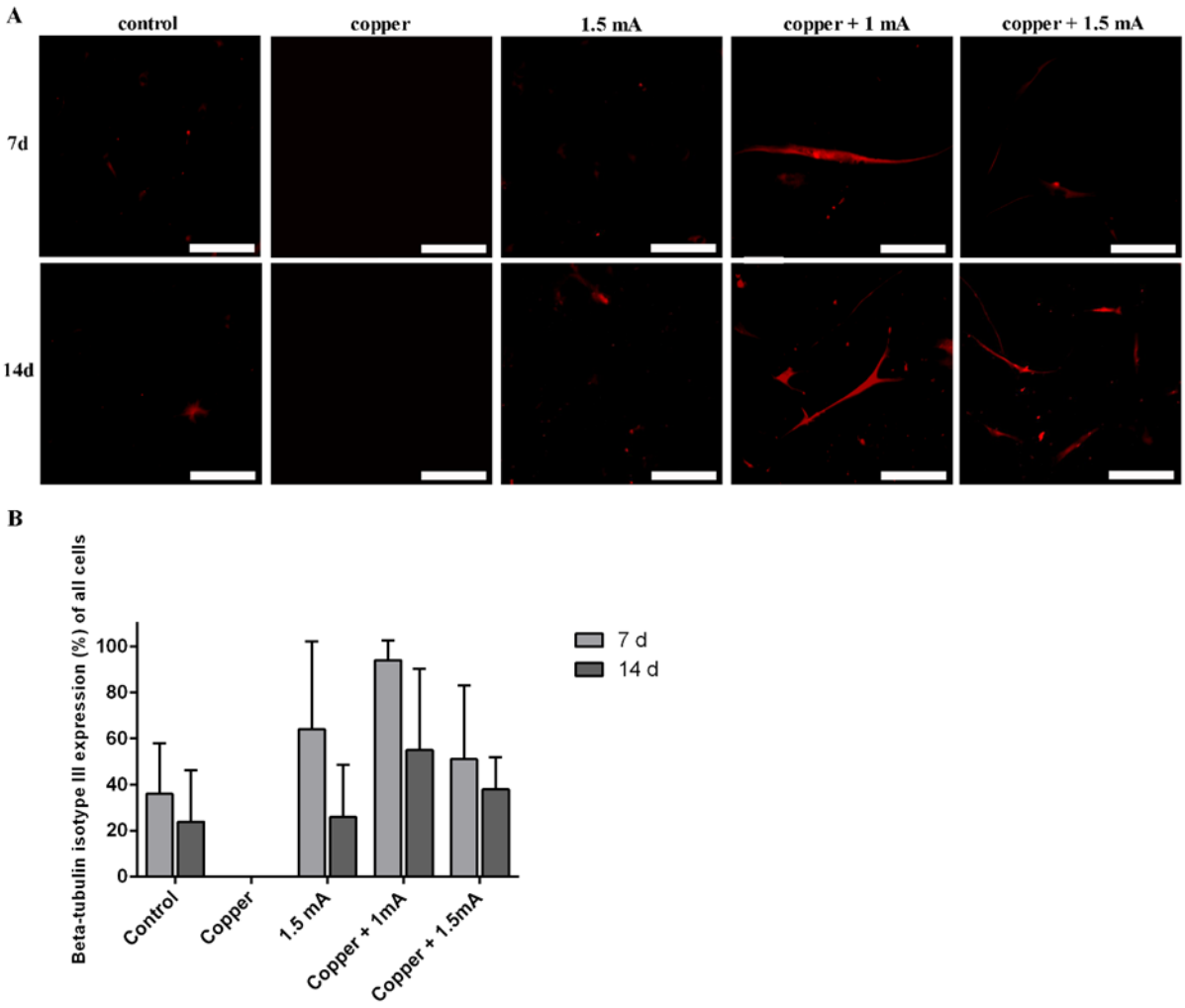

Figure 31. Fluorescent images (A) and graphs presenting the percentage of positive ADSC stained with anti-beta-tubulin isotype III neuronal antibody (B) at 7, and 14 days after stimulation of adhered cells. Scale bars are 100 µm. The data in graphs represent the mean ± SEM of triplicates.

A positive expression of MAP-2, a mature neuronal marker, was observed in the cells in suspension were stimulated with current alone or with both current and copper (Fig.

32). Between day 4 and day 14, the expression was increasing in these stimulation groups apart from the drop in expression in cells stimulated with Cu + 1 mA at day 7. Expression in all stimulation groups with current alone or both current and copper was highest at day 14 compared to the control. The highest expression was observed in cells stimulated with Cu + 1.5 mA. Control cells and cells stimulated with copper alone showed no MAP-2 expression in any time points.

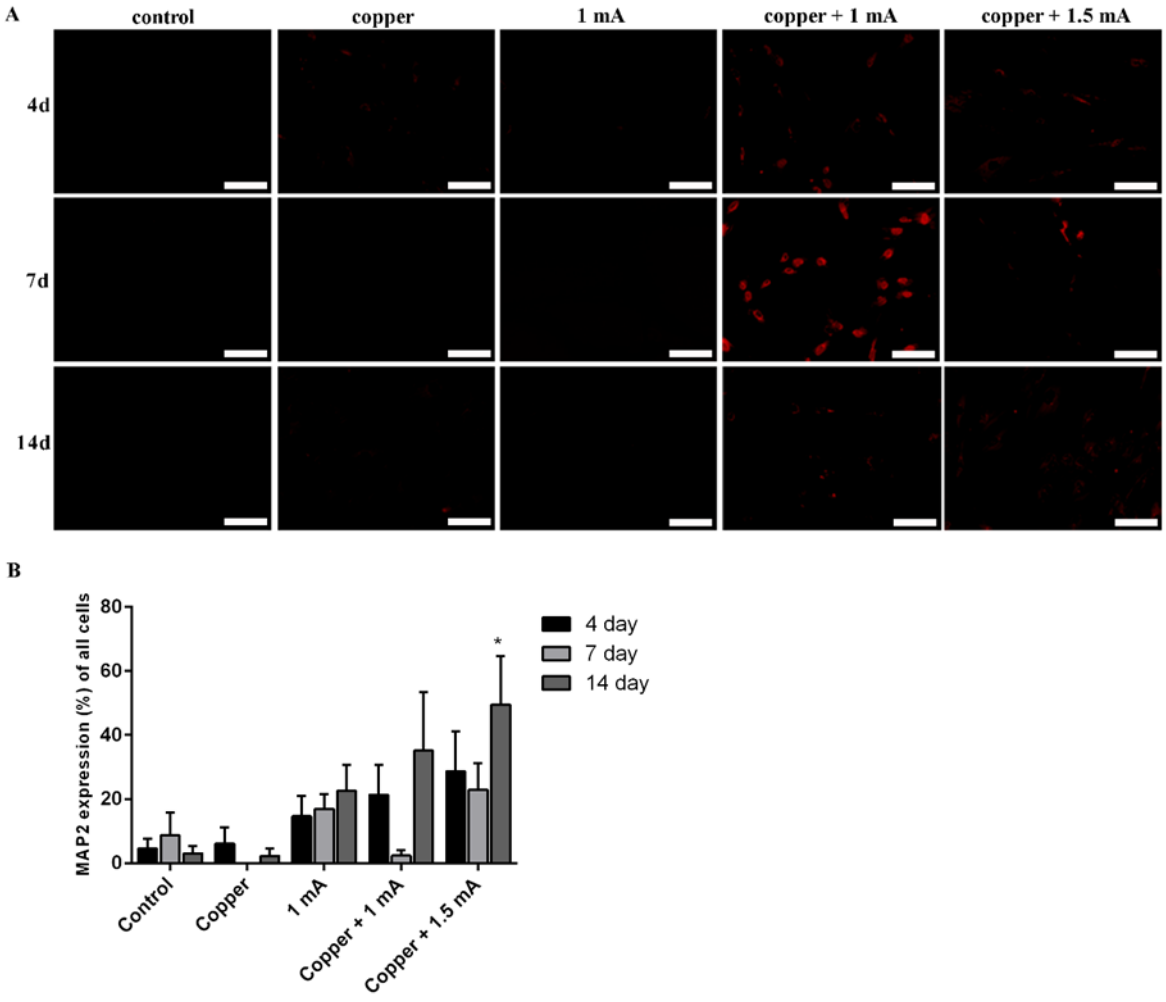

Figure 32. Fluorescent images (A) and graphs presenting the percentage of positive ADSC stained with anti-MAP2 neuronal antibody (B) at 4, 7, and 14 days when the cells were stimulated in suspension. Scale bars are 100 µm. The data in graphs represent the mean ± SEM of triplicates.

Shortly, only when ADSCs were stimulated with both copper and current (1 mA or 1.5 mA), there was a positive expression of both beta-tubulin isotype III and MAP-2 in immunohistochemical staining. Also the highest expressions of both antibodies were detected when the stimulation combined both copper and current.

4.7.2 Protein and mRNA expression

The western blot (WB) analysis showed increased levels of the neuronal protein beta-tubulin isotype III (46 kDa) in all of the experimental conditions at day 4 compared to the untreated control when the stimulation with copper was involved. The increase was highest when the ADSCs were stimulated with copper alone (Fig. 33). At day 7, the expression increased further within the cells stimulated with both current and copper. There was also a small increase in the expression in the cells stimulated with current only whereas in the copper alone stimulation, the expression had become almost negligible. At day 14, the beta-tubulin isotype III expression of copper + 1 mA had decreased to the same level as in the control and in other stimulation groups the expression was lower than in the control. The MAP-2 (239 kDa) protein expression at day 4 was higher in all of stimulation conditions compared to the untreated control except the current alone stimulation. At day 7, the expression had slightly decreased and there was no significant difference between the different stimulation conditions. At day 14, the expression had decreased more, being almost at the same level with the control.

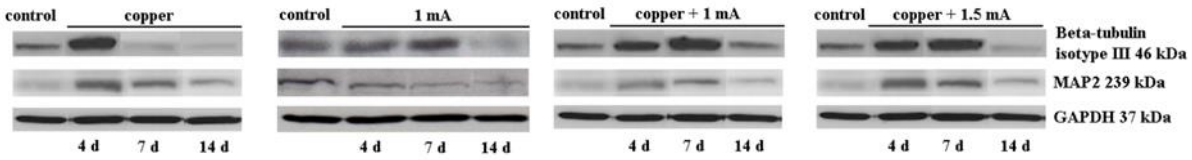

Figure 33. Neuron-specific protein expression of stimulated ADSCs. Western blot analysis showing the expression of the 46-kDa beta-tubulin isotype III protein, and the 239-kDa MAP-2 protein of the control cells and the stimulated cells at days 4, 7, and 14.

The stimulation of ADSCs with copper and current significantly increased the mRNA expression of beta-tubulin isotype III already at day 4 compared to the untreated control (figure 34 A). Also cells stimulated with current alone showed a small, non-significant increase in beta-tubulin isotype III expression. Increase in beta-tubulin isotype III expression was greatest when the ADSCs were stimulated with 1 mA current and a gradual Cu^{2+} release via electrolysis (Cu + 1 mA). At day 7, expression levels of cells stimulated with both copper and current increased even more, but then decreased by the day 14. The level stayed significantly higher than that of the control when the ADSCs were stimulated with both copper and 1 mA. When the cells were stimulated with copper or current alone, there was no significant increase in the expression levels except the 14 day expression of cell stimulated with 1 mA. The MAP-2 mRNA levels were significantly increased compared to the control when the cells were stimulated with both copper and 1 mA. The highest expression was seen at day 14 with copper + 1 mA whereas the other stimulation conditions did not show increase at any time points. (Fig.34 B).

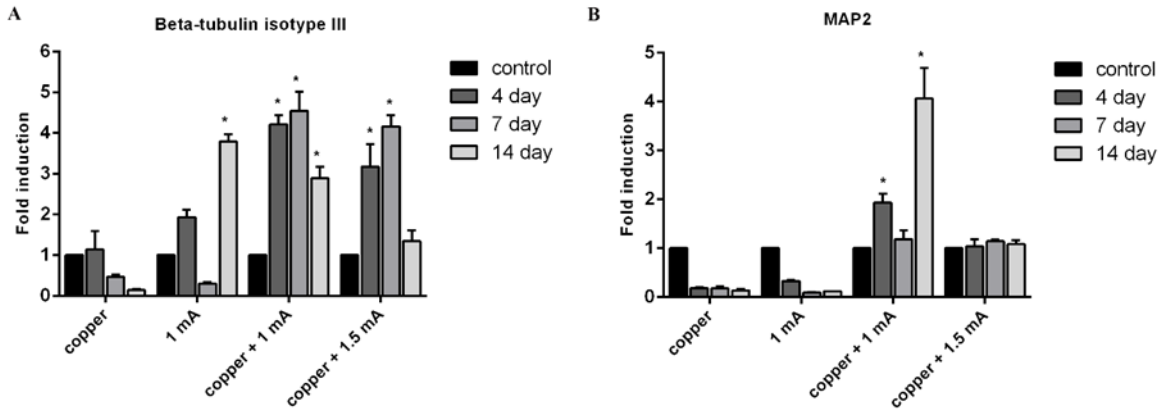

Figure 34. mRNA expression of neuron-specific markers in control ADSCs and stimulated ADSCs at days 4, 7, and 14. Induction of the gene expression of the neuronal markers (A) beta-tubulin isotype III and (B) MAP-2 was determined by real-time PCR using 18S as the control gene. The data represent the mean ± SEM of triplicates; the asterisk indicates $p < 0.05$ with respect to the control.

4.7.3 Comparison between cells from different donors

The above presented effect of electric current and copper on neuronal differentiation was observed when stimulating ADSCs from three different donors. The protein and mRNA expression results were thus an average of three biological and several technical replicates. There were some donor-to-donor variations detected. All the cells showed increase in the neuronal markers but cells from one of the donors (09/10) showed significantly less expression than the cells from the two other donors. The same phenomena was observed when stimulating cells both in suspension and as adhered, however, the expression of markers with the cells from this particular donor was even lower when stimulating cells in suspension.

5. Discussions

When a direct electric current (DC) was applied to the cell culture, several effects took place on the electrode, cellular and subcellular level. The current induced electrochemical reactions on the electrode/electrolyte interface and changed the cell morphology, proliferation, adhesion, and differentiation profile. These changes are discussed in the following subchapters.

5.1 Generation of reactive oxygen species and changes in pH

The cyclic voltammetry performed with the different electrode materials showed the boundaries for the reversible, capacitive region or the region for electrochemical, possibly irreversible reactions. For the ITO, the oxidation reactions, and thus the production of reactive oxygen (redox) species started at around 1.3 V. The potentials recorded during the stimulation were often higher than 1.3 V, however the cell culture medium includes a buffer thus some irreversible reactions are often not harmful to the cells. (Plonsey & Barr 2007) This was also noticed in the cell viability assessment which is discussed in the next chapter.

When the cells in suspension were stimulated with stainless steel electrodes with the layers of palladium, copper and platinum, the electrochemical reactions occurred

already at the very small positive voltages. The highest voltage recorded during the stimulation was 0.6 V and as the pure stainless steel electrodes were at the capacitive region until approximately 1.2 V and palladium and platinum are stable until around 0.9 V (Plonsey & Barr 2007), the redox species were generated mostly at the copper surface of the electrode and Cu^{2+} was released to the cell culture medium. Electric current is also know to change the local pH in the close vicinity of the electrode due to water electrolysis, which affects the stability of protein layers at the electrode and modifies the cell adhesion properties. (Guillaume-Gentil, Gabi, et al. 2011; Gabi et al. 2009) At the anode, there was a decrease and at the cathode, an increase of pH. The effect of changes in pH and generation of ROS on cell behavior is discussed in the following chapters.

5.2 Cell proliferation

5.2.1 Determining cell proliferation by electric impedance

The application of electric impedance-based setup was evaluated to detect the existence and number of viable cells inside a three-dimensional polylactide-96/4 (PLA96/4) scaffold based on the dielectric properties of the cells. At the here used frequency of 100 kHz, the cells behave as insulators, increasing the total impedance of the system. (Arndt et al. 2004) The accumulation of DNA was analyzed to estimate cellularity at the time points of 1, 7, 14, and 21 days together with the impedance measurements. Electrical impedance measurements could provide potential means to estimate numbers of live cells in 3D constructs noninvasively without expensive instrumentation. Even so, the method was highly sensitive to the various external factors. The most reliable information was obtained at day 1, when the measured impedance reflected the seeded cell number. However the impedance after day 1 in the scaffolds seeded with different cell number decreased despite the increasing DNA content and thus cell number. This suggests that variations in the composition and structure of the scaffold as well as in culture environment had more impact on measured impedance than the changes in the cell number. The biomaterial used here

was biodegradable in the biologic fluid, which may have changed the structure and composition of the scaffolds over culture and thereby interfered with the measured impedance.

5.2.2 The effect of electric stimulation to cell proliferation

The effect of applied current on cell proliferation was investigated in several different setups. When the cells were adhered directly on the electrode, the used current densities were considerably smaller than when the cells were not in a direct contact with the cells. In addition to having the cells adhered on the electrode or on a glass slide with the electrodes around them, the cells were also stimulated in suspension when there was also a constant mixing of the cell culture medium.

The cell proliferation was studied with the ADSCs 4, 7, and 14 days after the stimulation for one hour at the day 0 either as seeded on a glass slide or in a suspension. In both setups, the cells proliferated in the control conditions but the proliferation rates decreased especially when the cells were stimulated with the current only. It has been previously shown that stimulation of neural stem cells with biphasic current pulses increased the proliferation (Chang et al. 2011) but as in this thesis the monophasic current were used, there was a possibly harmful accumulation of charges and inhomogeneous distribution of redox species. In addition, the current densities were significantly higher than those used by Chang et al. who also showed that the proliferation rates decreased with the increase in current density. When the adhered ADSCs were stimulated with copper + 1.5 mA, cell number even decreased between days 4 and 14 days, however, this cannot be explained with the decrease in viability as the viability was affected only with the current of 10 mA and higher. In general, the proliferation of the ADSCs was less affected when the cells were stimulated in suspension compared to the stimulation of adhered cells. This can be due to the constant mixing of the cell suspension and thus the more homogeneous spreading of the redox species within the medium. The decrease in proliferation can be a result of several reasons; slow proliferation rates can be a sign of a low viability. In addition, the stem cells that differentiate, show lower proliferation rates, which is discussed in the chapter 6.4.

5.3 Cell morphology and viability

Exposing cells to electric current is known to induce cell death after a certain current threshold. Cathodic (negative) voltages usually trigger cell death through apoptosis whereas anodic (positive) voltages induce necrosis. Both anodic and cathodic voltages also cause changes to the cell morphology. (Haeri et al. 2012) The changes in morphology and viability as a result of the current stimulation was studied with both the ADSCs and C2C12s. The C2C12s were cultured directly on the electrode and their morphology started to change to more rounded with the applied current doses higher than 14 As/m^2 that was also related to the decrease in the cell viability. There was no decrease in viability below the 14 As/m^2 assessed immediately after the current exposure even with voltages as high as 1.8 V, thus the viability is rather related to the current dose than the voltage, at least within the voltage range used here. The acidic pH has been shown to directly induce cell death (Lee et al. 2011), therefore the decrease in cell viability was likely to be related to the change in the local pH due to the applied electric current, already demonstrated by Gabi et al. (Gabi et al. 2009). This effect is very local and takes place only in the close vicinity, less than 200 µm away from the electrode, and can explain also why the cells on the control electrodes showed no changes in their viability. Also the release of (metal) ions from the electrodes can cause both apoptosis and necrosis, and the effect is dependent on dose, time, cell type and the type of the (metal) ions (Haeri et al. 2012), and the effect can also be delayed. Current doses below 14 As/m^2 did not decrease the cell viability nor morphology instantly after the stimulation but the current doses of 11-14 As/m^2 resulted in cell death 24 hours after the stimulation. When the cells were exposed to high current doses of 30 As/m^2, many cells showed no rounding up but appeared spread on the substrate. This can be a sign of cells dying via necrosis instead of apoptosis where cells shrink and become more rounded. (Haeri et al. 2012)

Also the ADSCs were stimulated as adhered cells but without a direct contact to the electrode, therefore the used current densities and doses that had an effect on the viability were much higher compared to the stimulation of the C2C12s that were cultured directly on the electrode. ADSC viability was only affected at the current dose

of 17 000 As/m^2. As there was no mixing of the culture medium, also the distance of the cells from the stimulation electrodes had an influence on the cell viability; the closer the cells were to the working electrode where the Cu^{2+} was released to the culture medium, the more dead cells were detected. This leads to a conclusion that the concentration of Cu^{2+} and toxic redox species released in the medium due to electrolysis play a crucial role in the cell survival when the applied current doses are high enough. The amount of ROS released to the medium is proportional to the applied current dose as the amount of the measured intracellular ROS has shown to increase with the increase in the electric stimulation time (Sauer et al. 1999; Serena et al. 2009) and high amounts of ROS cause cell death (Simon et al. 2000). The viability of the ADSCs stimulated as suspension decreased around 20 % immediately after the stimulation, before the cells were seeded to the culture flasks and chamber slides but after the seeding, no cytoplasmic changes nor damage to the nucleus was detected which could be a sign of the lack of cell stress or death (Lu et al. 2004; Neuhuber et al. 2004).

In addition to the cell viability, also the morphology of the adhered ADSCs was affected by the current. The non-stimulated ADSCs maintained their adipose-like flat shape whereas the stimulated cells appeared more elongated even at day 14 after the stimulation. Stimulation of cells with an electric field is known to cause changes in their morphology due to actin cytoskeleton reorganization and membrane-cytoskeleton dissociation (I. a Titushkin & Cho 2009). It has been shown that ADSCs stimulated with a direct current elongate up to 145% of their original length within 2 hours (Tandon et al. 2009). Also orientation due to the electric stimulation has been demonstrated (Zhao et al. 2004; Tandon et al. 2009), however in this thesis only elongation and not orientation was observed even though the electrode location in relation to the cells was identical. The previously mentioned studies used the stimulation times of at least 2 hours compared to 1 hour used in this thesis. The ADSCs stimulated in suspension also showed elongation as long as 14 days after the stimulation. The elongation was observed always when the cells were stimulated with the current, both with and without copper. The cells stimulated with copper only maintained their adipose-like, spindle-shaped morphology.

Neither elongation nor orientation was observed with C2C12 cells while, due to the geometry of the stimulation electrode setup, the directionality was not supported by the electric field.

5.4 Cell adhesion

Alterations in the cell morphology and viability are often changing the properties of the cytoskeleton and the focal adhesion sites and therefore induce changes also in the cell adhesion to the substrate. The individual C2C12 cells were cultured directly on the ITO electrode and then detached by retracting the cantilever, while the corresponding force-distance curves were recorded. The adhesion in control conditions, without an applied current, was measured with two different FluidFM devices; a commercial and a custom-built one. There were no device-dependent differences detected in the measured adhesion forces. However, the advantage of the custom-built device was that it can move the cantilever up as far as 2 mm from the substrate whereas the commercial device can reach the detachment distance maximum of 50 µm. The measured maximum cell adhesion forces in control conditions were in good agreement with the values obtained earlier with the FluidFM, namely 473 ± 127 nN maximum adhesion forces for HeLa cells cultured on glass. (Potthoff et al. 2012)

Current doses smaller than 11 As/m^2 resulted in a small, nonsignificant increase in the maximum cell adhesion force. The decrease in the extracellular pH due to the applied current can be responsible for the effect (Tan et al. 2005; Paradise et al. 2011), but the positively charged current electrode itself may also result in higher cell adhesion forces according to the work of McNamee et al., who showed that positively charged particles give strong adhesive forces with melanoma cells (McNamee et al. 2006). Also small amounts of ROS can alter, and usually increase the cell adhesion. (Sauer et al. 1999; Huo et al. 2009)

Cells stimulated with current doses of 11-16 As/m^2 had a more round morphology compared to the control and smaller current doses and the round morphology was associated with smaller adhesion forces compared to that of the control cells. At

current doses higher than 16 As/m^2 the maximum adhesion force was significantly higher compared to the control. The cell viability at these current doses was less than 40 % and the increase in adhesion forces can be correlated with the cell death. Some of the cells exposed to the high current doses maintained a rather spread morphology instead of rounding up, although appearing dead. This can be a sign of the cell dying via necrosis instead of apoptosis (Haeri et al. 2012) which could be related to the high adhesion forces.

There was a significant increase also in the detachment distance with the current doses above 11 As/m^2 and at the highest current doses the detachment distance increased further, sometimes even exceeding the maximum cantilever retraction length possible with the commercial device. In these cases, when the cantilever was moved parallel to the substrate, away from the cell attachment site, cells could sometimes be stretched as long as a few hundreds of microns. The reason for the significantly longer detachment distance should originate from other, presumably dynamic properties like alterations in the dynamics of actin reorganization, which is one of the consequences of the increased calcium concentration (Titushkin & Cho 2009) resulting also in smaller adhesion forces (Alberts et al. 2008).

In order to find out if the changes in adhesion forces were correlated with the alterations in the focal adhesion sites, the cells were stained against vinculin that is one of the most prominent part of focal adhesion complex. It is known that vinculin is important for adhesive strength. Increasing the external or internal forces acting on the cell results in the assembly of the focal adhesions, while a decrease in the forces results in disassembled or shrunk focal adhesions. (Gallant et al. 2005) As the current dose reached 15 As/m^2 and cell morphology started to become more rounded, less clear vinculin structures were observed, while at even higher current doses when cell morphology became spherical, also the vinculin structures had disassembled and diffused throughout the cell body, a sign of the cells dying via necrosis with an applied high anodic voltages (Haeri et al. 2012). The loss of focal adhesions has been also associated with the overexpression of superoxide dismutase due to the high amounts of ROS. (Connor et al. 2007)

In addition to the C2C12 cell adhesion and detachment on an electrode, also the ADSC adhesion to a three-dimensional scaffold was studied under an applied electric current. In the measurement setup, a non-conductive polymer scaffold was surrounded with mesh electrodes. In the control conditions without an applied current, the cells were able to migrate through the mesh surrounding the scaffold and further adhere to the scaffold. When an electric current was applied to the mesh, the local pH in the close vicinity of the mesh most probably decreased (Gabi et al. 2009; Guillaume-Gentil, Semenov, et al. 2011) and the majority of cells could no longer adhere to the mesh and further to the scaffold. With higher current densities, this effect was further enhanced. The poor adherence in the mesh correlated with the absence of the cells within the scaffold. Electric current also altered the migration depth into the scaffold; the higher the current, the more the cells stayed on the top layers of the scaffold. When the mesh pores were bigger than the cells, the cells could pass through and migrate into the scaffold despite the current that was changing the pH only in a very close vicinity of the electrode. In general, the migration of the cells through the mesh prior to the adhesion to the scaffold is most likely due to simple diffusion and not an active process that requires adhesion to the mesh.

5.5 Stem cell differentiation

The ADSCs were stimulated with currents of 1 mA and 1.5 mA that correspond to current densities of 4 A/m^2 and 6 A/m^2, current doses of 2.88 mAs/m^2 and 4.32 mAs/m^2, respectively, and electric field strengths of 35 mV/mm and 53 mV/mm in Cu + 1 mA and Cu + 1.5 mA stimulations with copper electrodes, and 155 mV/mm in 1 mA stimulation with platinum electrodes. The expression of two markers, beta-tubulin isotype III and MAP-2, was assessed in mRNA and protein level. The two markers were chosen because beta-tubulin isotype III is a characteristic marker for immature neurons that has been previously used in analysis of neurogenic differentiation of ADSCs. (Cardozo et al. 2012) MAP-2 is expressed at the later time points by the mature neurons. (Abrous et al. 2005)

Only cells stimulated with both copper and current showed both the morphological changes typical to neuron-like cells (chapter 6.2) and the beta-tubulin isotype III and MAP-2 expression at mRNA and protein level. At mRNA level the highest expression of beta-tubulin isotype III was detected at day 7 and in immunohistochemistry at protein level the highest expression was seen at day 14. For the MAP-2 expression, at the mRNA level, high MAP-2 expression was observed only when the cells were stimulated with copper and 1 mA. Beta-tubulin isotype III and MAP-2 measured by WB showed a higher expression when the cells were stimulated with copper and the combination of copper and current compared to control and the cells stimulated with current alone.

There were some differences of the beta-tubulin isotype III and MAP-2 expression between the immunostaining and WB. Immunostaining showed high expression at day 14 when the expression levels in WB had already decreased, could be explained by the cell proliferation; the relative number of non-differentiated cells was increasing in the culture flask and as WB shows the total expression of protein, the expression levels were apparently decreased. Additionally, it is known that only a small proportion of ADSCs can differentiate into neurons (Jiang et al. 2003) and therefore, by WB, lower expression of neuronal markers was detected compared to the immunostaining where we looked at the neuron-positive cells.

Based on the results presented in this chapter, there is a clear indication that the differentiation of ADSCs toward the neuronal lineages can be triggered by using combination of an electric current and continued copper stimulation. Electric fields are known to be related to the neuronal differentiation of embryonic, neural and mesenchymal stem cells (Ariza et al. 2010; Matos & Cicerone 2010; Thrivikraman et al. 2014; Yamada et al. 2007) The stimulation of hippocampal neural progenitor cells with a continuous DC electric field of 437 mV/mm, corresponding to a current of 3.38 mA, increased the neural differentiation tendency. (Ariza et al. 2010) In another study, human mesenchymal stem cells were differentiated towards neuron-like cells using a much weaker, continuous DC electric field of 10 mV/mm. (Thrivikraman et al. 2014)

It is thus possible that the differentiation process can take place also when stimulating cells with electric field only, however, the upregulation of beta-tubulin isotype III, a

marker for immature neurons, was seen only after 14 days of culture, compared to 4 days when using electric field and copper together. The mature neuronal marker, MAP-2, showed no increase in expression levels within the 14 days of culture when the ADSCs were stimulated with current alone. Copper is well known to play an important role in brain development. (Madsen & Gitlin 2007; Nalbandyan 1983) High amounts of copper are also stored in the synaptic terminals of central neurons (Sato et al. 1994), and it has been shown that copper can modify neuronal excitability (Horning & Trombley 2001)

Rodrigues et al. showed that an increase in the extracellular concentration of copper modifies the proliferation and differentiation of mesenchymal stem cells *in vitro*. Their results show that the addition of copper to a culture of MSCs in osteogenic or adipogenic differentiation media decreased the proliferation and promoted the osteogenic or adipogenic differentiation of MSCs, respectively. The authors concluded that copper plays a role either in the commitment of the MSCs toward a specific differentiation pathway or in the maturation of the chosen cell lineage. (Rodriguez et al. 2002) Monson et al showed that phosphatidylserine (PS) binds Cu^{2+} with very high affinity. (Monson et al. 2012) PS is a phospholipid that is found in the cell membrane and is particularly enriched in neuronal membranes (Kim 2007) Thus, the stimulation of ADSCs with copper may result in Cu^{2+} binding to the PS in the cell membrane to initiate the commitment step in the differentiation toward the neuronal lineage. It is possible that the external electric field is enabling a more efficient intake of Cu^{2+} into the cell. This may be due to the reassembly or redistribution of the phospholipid PS, or generally phospholipids by electric field, reported in several studies. (Zhao et al. 2002; Poo 1981) Electric stimulation can also result in displacement of membrane proteins (Poo 1981), such as copper transporter Ctr1 and thus influence the copper intake.

Stimulating ADSCs with both copper and current seems to induce the highest and fastest expression of the two neuronal markers. Here used current densities and consequent Cu^{2+} concentrations are high enough to induce the neuron-like differentiation of ADSCs but no clear causality between the two current densities was observed. However, differentiation of functional neurons is a complicated process and

neuron-like morphology and expression of neuronal markers beta-tubulin isotype III and MAP-2 alone does not prove that the ADSCs become functional neurons. Therefore, in this study it is shown that stimulation with electric currents and copper induces neuron-like changes in the cell morphology as well as gene and protein expression but in the future, the neuron functionality has to be verified in order to confirm that the ADSCs can differentiate into mature neurons. The in vitro experiments offer information regarding growth factor-free differentiation of ADSC to neuron-like cells which can be a base for further pre-clinical studies. Further animal studies are required to evaluate the tissue response, nerve regeneration and functionality of these neuron-like cells in vivo.

5.6. The effect of the stimulation parameters and the cell type

The effect of electric current on cells is highly dependent on the stimulation parameters such as such as the polarity, magnitude and stimulation time (Balint et al. 2013), stimulation conditions and the cell type (Titushkin et al. 2004; Rajnicek 2011; McCaig et al. 2009). In the washing assay performed, the C2C12 cell viability was significantly less affected by the applied current than that of the ADSC. This could indicate that the stem cells are more vulnerable to the current than the differentiated cells. It has been shown previously that the actin fibers in mesenchymal stem cells (MSCs) are more susceptible to an applied electric field than those in osteoblasts, resulting in more prominent changes in cell elasticity of MSCs compared to the osteoblasts. (Titushkin & Cho 2009) When the stem cell differentiation was studied, also some donor-to-donor variations were detected.

The cells cultured directly on the electrode were able to sustain much smaller current densities and doses compared to the cells that were not in a direct contact with the cells in the terms of the cell viability. When the cells are not in contact with the electrode, they are most probably affected only by the ROS generated by the electric current, not the direct effect of the current on for instance cell membrane ion channels or the decrease of pH close to the electrode. The cell viability was rather correlated

with the applied current dose than the potential while even high voltages did not influence the cell viability as long as the current dose was below a certain threshold. When the threshold was reached, also the current density and the exposure time played a role. The cell adhesion was more affected by the small current density applied for a long time than a higher current density applied for a shorter time, possibly due to the accumulation of ROS.

7. Conclusions

In this work, the effect of electric current on cell proliferation, morphology, viability, adhesion, and stem cell differentiation was investigated. The main conclusions and most important findings were the following:

I. Cell morphology and viability can be altered by the applied electric current, and it was possible to define a current dose threshold for these changes to start occurring, where the threshold is dependent on the cell type.
II. Adhesive and mechanical properties of cells can be manipulated by the use of electric currents, and the adhesion forces can be quantified very precisely with a method called FluidFM.
III. Stimulation with electric fields combined with a sustained release of copper could provide a feasible, non-expensive, growth factor-free method for the differentiation of ADSCs toward the neuronal lineage indicated by morphological changes and upregulation of neuron-specific genes and proteins.

When an electric current was applied to the cell culture, the cell spreading area decreased monotonously with increasing current doses, however, small current doses did not result in differences in cell adhesion forces. Only current doses above 11 As/m^2 that also initiated more drastic changes in cell morphology, viability, cellular structure, changed the cell adhesion strength. The observed differences, eventually leading to cell death towards higher doses, might originate from both the decrease in pH and the generation of reactive oxygen species. Electrical stimulation could provide a controlled,

well-defined method to release ROS for stem cells and find thresholds and optimal conditions for the different cellular behaviors.

The electrical stimulation, combined with a controlled release of Cu^{2+} induced also stem cell differentiation toward the neuronal lineage with elongation of the cells and the upregulation of neuron-specific genes and proteins. However, differentiation of functional neurons is a complicated process and in the future, the neuron functionality has to be verified in order to confirm that the ADSCs can differentiate into mature neurons.

Further *in vitro* experiments for instance with a microelectrode array or *in vivo* animal studies are required to evaluate the tissue response, nerve regeneration and functionality of these neuron-like cells in vivo. Nevertheless, the induction of the neuronal differentiation of ADSCs by electric field and copper may offer a novel approach for stem cell differentiation and may be a useful tool for safe stem cell-based therapeutic applications.

References

Abrous, D.N., Koehl, M. & Moal, M.L.E., 2005. Adult Neurogenesis : From Precursors to Network and Physiology. *Physiol. Rev*, (322), pp.523–569.

Alberts, B. et al., 2008. *Molecular biology of the cell, 5th edition*

Anghileri, E. et al., 2008. Neuronal differentiation potential of human adipose-derived mesenchymal stem cells. *Stem cells and development*, 17(5), pp.909–16.

Ariza, C.A. et al., 2010. The influence of electric fields on hippocampal neural progenitor cells. *Stem cell reviews*, 6(4), pp.585–600.

Arndt, S., J. Seebach, K. Psathaki, H. J. Galla, and J. Wegener. Bioelectrical impedance assay to monitor changes in cell shape during apoptosis*. Biosens. Bioelectron*. 19:583-94, 2004.

Bagnaninchi, P. O., M. Dikeakos, T. Veres, and M. Tabrizian. Complex permittivity measurement as a new noninvasive tool for monitoring in vitro tissue engineering and cell signature through the detection of cell proliferation, differentiation, and pretissue formation*. IEEE Trans Nanobioscience*. 3:243-50, 2004.

Bagnaninchi, P. O. Combined impedance spectroscopy and fourier domain optical coherence tomography to monitor cells in three-dimensional structures*. Int J Artif Organs*. 33:238-43, 2010.

Bagnaninchi, P. O. and N. Drummond. Real-time label-free monitoring of adipose-derived stem cell differentiation with electric cell-substrate impedance sensing. *Proc Natl Acad Sci U S A*. 108:6462-7, 2011.

Bai, H. et al., 2004. DC electric fields induce distinct preangiogenic responses in microvascular and macrovascular cells. *Arteriosclerosis, Thrombosis, and Vascular Biology*, 24(7), pp.1234–1239.

Balint, R., Cassidy, N. & Cartmell, S., 2013. Electrical Stimulation: A Novel Tool for Tissue Engineering. *Tissue Engineering Part B Rev*, 19(1), pp.48–57.

Barker, R. a. & de Beaufort, I., 2013. Scientific and ethical issues related to stem cell research and interventions in neurodegenerative disorders of the brain. *Progress in Neurobiology*, 110, pp.63–73.

Berrier, A.L. & Yamada, K.M., 2007. Cell-Matrix Adhesion. *Journal of cellular physiology*, 213(3), pp.565–573.

Birkaya, B. & Aletta, J.M., 2005. NGF promotes copper accumulation required for optimum neurite outgrowth and protein methylation. *Journal of neurobiology*, 63(1), pp.49–61.

Blumenthal, N.C. et al., 1997. Effects of low-intensity AC and/or DC electromagnetic fields on cell attachment and induction of apoptosis. *Bioelectromagnetics*, 18(3), pp.264–72.

Borgens, R. Ben, 2011. Can Applied Voltages Be Used to Produce Spinal Cord Regeneration and Recovery in Humans ? In *The Physiology of Bioelectricity in Development, Tissue Regeneration, and Cancer*. pp. 233–266.

Cardozo, A.J., Gómez, D.E. & Argibay, P.F., 2012. Neurogenic differentiation of human adipose-derived stem cells: relevance of different signaling molecules, transcription factors, and key marker genes. *Gene*, 511(2), pp.427–36.

Chang, K.-A. et al., 2011. Biphasic electrical currents stimulation promotes both proliferation and differentiation of fetal neural stem cells. *PloS one*, 6(4), p.e18738.

Cho, M.R., 2002. A review of electrocoupling mechanisms mediating facilitated wound healing. *IEEE Transactions on Plasma Science*, 30(4), pp.1504–1515.

Cho, M.R. et al., 1994. Induced redistribution of cell surface receptors in AC electric fields. *The FASEB journal*, 8, pp.771–776.

Choi, S.A. et al., 2012. Human adipose tissue-derived mesenchymal stem cells: characteristics and therapeutic potential as cellular vehicles for prodrug gene therapy

against brainstem gliomas. *European journal of cancer (Oxford, England : 1990)*, 48(1), pp.129–37.

Connor, K.M. et al., 2007. Manganese superoxide dismutase enhances the invasive and migratory activity of tumor cells. *Cancer Research*, 67(21), pp.10260–10267.
Davey, C. L. and D. B. Kell. The influence of electrode polarization on dielectric spectra, with special reference to capacitive biomass measurements i. Quantifying the effects on electrode polarization of factors likely to occur during fermentations. *Bioelectroch. Bioener.* 46:91–103, 1998.

Dziong, D., P. O. Bagnaninchi, R. E. Kearney, and M. Tabrizian. Nondestructive online in vitro monitoring of pre-osteoblast cell proliferation within microporous polymer scaffolds. *IEEE Trans Nanobioscience*. 6:249-58, 2007.

Dörig, P. et al., 2010. Force-controlled spatial manipulation of viable mammalian cells and micro-organisms by means of FluidFM technology. *Applied Physics Letters*, 97(2), p.023701.

Gabi, M. et al., 2009. Influence of applied currents on the viability of cells close to microelectrodes. *Integrative biology : quantitative biosciences from nano to macro*, 1(1), pp.108–15.

Gallant, N.D., Michael, K.E. & Garcia, A.J., 2005. Cell Adhesion Strengthening: Contributions of Adhesive Area, Integrin Binding, and Focal Adhesion Assembly. *Molecular biology of the cell*, 16, pp.4329–4340.

Giaver, I. and C. Keese. Use of electric fields to monitor the dynamical aspect of cell behavior in tissue culture. *IEEE Trans. Biomedical Engineering* 2:242-247, 1986.

Guillaume-Gentil, O., Gabi, M., et al., 2011. Electrochemically switchable platform for the micro-patterning and release of heterotypic cell sheets. *Biomedical microdevices*, 13(1), pp.221–30.

Guillaume-Gentil, O., Semenov, O. V, et al., 2011. pH-controlled recovery of placenta-derived mesenchymal stem cell sheets. *Biomaterials*, 32(19), pp.4376–84.

Guillaume-Gentil, O., Zambelli, T. & Vorholt, J. a, 2014. Isolation of single mammalian cells from adherent cultures by fluidic force microscopy. *Lab on a chip*, 14(2), pp.402–14. A

Gumus, A. et al., 2010. Control of cell migration using a conducting polymer device. *Soft Matter*, 6(20), p.5138.

Gunja, N.J. & Hung, C.T., 2011. Effects of DC Electric Fields on Migration of Cells of the Musculoskeletal System. In *The Physiology of Bioelectricity in Development, Tissue Regeneration, and Cancer*. pp. 185–200.

Haeri, M. et al., 2012. Electrochemical control of cell death by reduction-induced intrinsic apoptosis and oxidation-induced necrosis on CoCrMo alloy in vitro. *Biomaterials*, 33(27), pp.6295–304.

Haremaki, T. et al., 2007. Vertebrate Ctr1 coordinates morphogenesis and progenitor cell fate and regulates embryonic stem cell differentiation. *Proceedings of the National Academy of Sciences of the United States of America*, 104(29), pp.12029–34.

Hart, F.X., 2006. Integrins may serve as mechanical transducers for low-frequency electric fields. *Bioelectromagnetics*, 27(6), pp.505–508.

Hart, F.X., 2011. Investigation Systems to Study the Biological Effects of Weak Physiological Electric Fields. In *The Physiology of Bioelectricity in Development, Tissue Regeneration, and Cancer*. pp. 17–38.

Hentze, H. et al., 2009. Teratoma formation by human embryonic stem cells: evaluation of essential parameters for future safety studies. *Stem cell research*, 2(3), pp.198–210.

Horning, M.S. & Trombley, P.Q., 2001. Zinc and Copper Influence Excitability of Rat Olfactory Bulb Neurons by Multiple Mechanisms Zinc and Copper Influence Excitability of Rat Olfactory Bulb Neurons by Multiple Mechanisms. *J Neurophysiol*, (86), pp.1652–1660.

Hronik-tupaj, M. & Kaplan, D.L., 2012. A Review of the Responses of Two- and Three-Dimensional Engineered Tissues to Electric Fields. *Tissue Engineering Part B Rev*, 00(00), pp.1–14.

Hunt, D.M., 1980. Copper and neurological function. *Ciba Foundation symposium*, 79, pp.247–66.

Huo, Y. et al., 2009. Reactive oxygen species (ROS) are essential mediators in epidermal growth factor (EGF)-stimulated corneal epithelial cell proliferation, adhesion, migration, and wound healing. *Experimental eye research*, 89(6), pp.876–886.

Jang, S. et al., 2010. Functional neural differentiation of human adipose tissue-derived stem cells using bFGF and forskolin. *BMC cell biology*, 11, p.25.

Jiang, Y. et al., 2003. Neuroectodermal differentiation from mouse multipotent adult progenitor cells. *Proceedings of the National Academy of Sciences of the United States of America*, 100 Suppl (20), pp.11854–60.

Kendall, K., Kendall, M. & Rehfeldt, F., 2011. *Adhesion of Cells, Viruses and Nanoparticles*, Dordrecht: Springer Netherlands.

Khademhosseini, A., Vacanti, J.P. & Langer, R., 2009. Progress in tissue engineering.

Scientific American, 300(5), pp.64–71.

Khatib, L., Golan, D.E. & Cho, M., 2004. Physiologic electrical stimulation provokes intracellular calcium increase mediated by phospholipase C activation in human osteoblasts. *The FASEB journal : official publication of the Federation of American Societies for Experimental Biology*, 18(15), pp.1903–1905.

Kim, H.-Y., 2007. Novel metabolism of docosahexaenoic acid in neural cells. *The Journal of biological chemistry*, 282(26), pp.18661–5.

Krampera, M. et al., 2007. Induction of neural-like differentiation in human mesenchymal stem cells derived from bone marrow, fat, spleen and thymus. *Bone*, 40(2), pp.382–90.

Lebonvallet, N. et al., 2012. Characterization of neurons from adult human skin-derived precursors in serum-free medium : a PCR array and immunocytological analysis. *Experimental dermatology*, 21(3), pp.195–200.

Lee, G.H. et al., 2011. An acidic pH environment increases cell death and pro-inflammatory cytokine release in osteoblasts: The involvement of BAX Inhibitor-1. *International Journal of Biochemistry and Cell Biology*, 43(9), pp.1305–1317.

Levin, M., 2011. Endogenous Bioelectric Signals as Morphogenetic Controls of Development, Regeneration, and Neoplasm. In *The Physiology of Bioelectricity in Development, Tissue Regeneration, and Cancer*. pp. 39–89.

Li, X. & Kolega, J., 2002. Effects of direct current electric fields on cell migration and actin filament distribution in bovine vasclar endothelial cells. *Journal of Vascular Research*, 39(391), pp.391–404.

Lindroos, B. et al., 2009. Serum-free, xeno-free culture media maintain the proliferation rate and multipotentiality of adipose stem cells in vitro. *Cytotherapy*, 11(7), pp.958–72.

Lu, P., Blesch, A. & Tuszynski, M.H., 2004. Induction of bone marrow stromal cells to neurons: differentiation, transdifferentiation, or artifact? *Journal of neuroscience research*, 77(2), pp.174–91.

Madsen, E. & Gitlin, J.D., 2007. Copper and iron disorders of the brain. *Annual review of neuroscience*, 30, pp.317–37.

Markx, G. and C. Davey. The dielectric properties of biological cells at radiofrequencies: Applications in biotechnology. *Enzyme and Microbial Technology*. 25 161–171, 1999.

Matos, M. a & Cicerone, M.T., 2010. Alternating current electric field effects on neural stem cell viability and differentiation. *Biotechnology progress*, 26(3), pp.664–70.

McCaig, C.D. et al., 1994. Growing nerves in an electric field. *Neuroprotocols*, 4, pp.134–141.

McCaig, C.D., Song, B. & Rajnicek, A.M., 2009. Electrical dimensions in cell science. *Journal of cell science*, 122(Pt 23), pp.4267–76.

McNamee, C.E., Pyo, N. & Higashitani, K., 2006. Atomic force microscopy study of the specific adhesion between a colloid particle and a living melanoma cell: Effect of the charge and the hydrophobicity of the particle surface. *Biophysical journal*, 91(5), pp.1960–1969.

Monson, C.F. et al., 2012. Phosphatidylserine reversibly binds Cu2+ with extremely high affinity. *Journal of the American Chemical Society*, 134(18), pp.7773–9.

Nalbandyan, R.M., 1983. An Overview Copper in brain. *Neurochemical Research*, 8(10).

Neuhuber, B. et al., 2004. Reevaluation of in vitro differentiation protocols for bone marrow stromal cells: disruption of actin cytoskeleton induces rapid morphological changes and mimics neuronal phenotype. *Journal of neuroscience research*, 77(2), pp.192–204.

Nuccitelli, R., 2011. Measuring Endogeneous Electric Fields. In *The Physiology of Bioelectricity in Development, Tissue Regeneration, and Cancer*. pp. 1–15.

Nuccitelli, R., 1988. Physiological Electric Fields can Influence Cell Motility, Growth, and Polarity. *Advances in Molecular and Cell Biology*, 2(C), pp.213–233.

Paradise, R.K., Lauffenburger, D.A. & Van Vliet, K.J., 2011. Acidic extracellular pH promotes activation of integrin α(v)β(3). *PloS one*, 6(1), p.e15746.

Pliquett, U. F. and K. H. Schoenbach. Changes in electrical impedance of biological matter due to the application of ultrashort high voltage pulses*. IEEE Transactions on Dielectric and Electric Insulation*. 16:1273-1279, 2009.

Plonsey, R. & Barr, R.C., 2007. *Bioelectricity - A quantitative Approach*,

Poo, M., 1981. In situ electrophoresis of membrane components. *Annual review of biophysics and bioengineering*, 10, pp.245–76.

Potthoff, E. et al., 2012. Rapid and serial quantification of adhesion forces of yeast and Mammalian cells. *PloS one*, 7(12), p.e52712.

Potthoff, E. et al., 2014. Toward a rational design of surface textures promoting endothelialization. *Nano letters*, 14(2), pp.1069–79.

Pullar, C.E., 2011. Physiologica Electric Fields Can Direct Keratinocyte Migration and Promote Healing in Chronic Wounds. In *The Physiology of Bioelectricity in Development, Tissue Regeneration, and Cancer*. pp. 137–153.

Rajnicek, A.M., 2011. Neuronal Growth Cone Guidance by Physiological DC Electric Fields. In *The Physiology of Bioelectricity in Development, Tissue Regeneration, and Cancer*. pp. 201–231.

Rodriguez, J.P., Rios, S. & Gonzales, M., 2002. Modulation of the Proliferation and Differentiation of Human Mesenchymal Stem Cells by Copper. *Journal of cellular biochemistry*, 100, pp.92–100.

Ross, S.M., 1990. Combined Dc and ELF Magnetic-Fields Can Alter Cell Proliferation. *Bioelectromagnetics*, 11(1), pp.27–36.

Sader, J.E., Chon, J.W.M. & Mulvaney, P., 1999. Calibration of rectangular atomic force microscope cantilevers. *Review of Scientific Instruments*, 70(10), pp.3967–3969.

Safford, K.M. et al., 2002. Neurogenic differentiation of murine and human adipose-derived stromal cells. *Biochemical and biophysical research communications*, 294(2), pp.371–9.

Sanchez-Ramos, J. et al., 2000. Adult bone marrow stromal cells differentiate into neural cells in vitro. *Experimental neurology*, 164(2), pp.247–56.

Sato, M. et al., 1994. Localization of copper to afferent terminals in rat locus ceruleus, in contrast to mitochondrial copper in cerebellum. *Journal of Histochemistry & Cytochemistry*, 42(12), pp.1585–1591.

Sauer, H. et al., 1999. Effects of electrical fields on cardiomyocyte differentiation of embryonic stem cells. *Journal of cellular biochemistry*, 75(4), pp.710–23.

Serena, E. et al., 2009. Electrical stimulation of human embryonic stem cells: cardiac differentiation and the generation of reactive oxygen species. *Experimental cell research*, 315(20), pp.3611–9.

Simon, H.-U., Haj-Yehia, A. & Levi-Schaffer, F., 2000. Role of reactive oxygen species (ROS) in apoptosis induction. *Apoptosis*, 5, pp.415–418.

Sun, S. et al., 2007. Physical manipulation of calcium oscillations facilitates osteodifferentiation of human mesenchymal stem cells. *FASEB journal : official publication of the Federation of American Societies for Experimental Biology*, 21(7), pp.1472–80.

Sun, S., Titushkin, I. & Cho, M., 2006. Regulation of mesenchymal stem cell adhesion

and orientation in 3D collagen scaffold by electrical stimulus. *Bioelectrochemistry (Amsterdam, Netherlands)*, 69(2), pp.133–41.

Tan, J. et al., 2005. Improved cell adhesion and proliferation on synthetic phosphonic acid-containing hydrogels. *Biomaterials*, 26(17), pp.3663–3671.

Tandon, N. et al., 2009. Alignment and elongation of human adipose-derived stem cells in response to direct-current electrical stimulation. *Conference proceedings : ... Annual International Conference of the IEEE Engineering in Medicine and Biology Society. IEEE Engineering in Medicine and Biology Society. Conference*, 2009, pp.6517–21.

Taubenberger, A. V, Hutmacher, D.W. & Muller, D.J., 2014. Single-cell force spectroscopy, an emerging tool to quantify cell adhesion to biomaterials. *Tissue engineering. Part B, Reviews*, 20(1), pp.40–55.

Thrivikraman, G., Madras, G. & Basu, B., 2014. Intermittent electrical stimuli for guidance of human mesenchymal stem cell lineage commitment towards neural-like cells on electroconductive substrates. *Biomaterials*, 35(24), pp.6219–6235.

Titushkin, I. et al., 2011. Stem Cell Physiological Responses to Noninvasive Electrical Stimulation. In *The Physiology of Bioelectricity*. pp. 91–120.

Titushkin, I. a & Cho, M.R., 2009. Controlling cellular biomechanics of human mesenchymal stem cells. *Conference proceedings : ... Annual International Conference of the IEEE Engineering in Medicine and Biology Society. IEEE Engineering in Medicine and Biology Society. Conference*, 2009, pp.2090–3.

.

Titushkin, I. & Cho, M., 2009. Regulation of cell cytoskeleton and membrane mechanics by electric field: role of linker proteins. *Biophysical journal*, 96(2), pp.717–28.

Titushkin, I.A., Rao, V.S. & Cho, M.R., 2004. Mode- and Cell-Type Dependent Calcium Responses Induced by Electrical Stimulus. *IEEE Transactions on Plasma Science*, 32(4), pp.1614–1619.

Ulrich, H. & Majumder, P., 2006. Neurotransmitter receptor expression and activity during neuronal differentiation of embryonal carcinoma and stem cells: from basic research towards clinical applications. *Cell proliferation*, 39(4), pp.281–300.

Wang, E. et al., 2003. Bi-directional migration of lens epithelial cells in a physiological electrical field. *Experimental Eye Research*, 76(1), pp.29–37.

Wang, E. et al., 2011. Electrical Control of Angiogenesis. In *The Physiology of Bioelectricity in Development, Tissue Regeneration, and Cancer*. pp. 155–175.

Wang, E. et al., 2005. Electrical inhibition of lens epithelial cell proliferation: an additional factor in secondary cataract? *The FASEB journal : official publication of the Federation of American Societies for Experimental Biology*, 19(7), pp.842–844.

Weiser, T. & Wienrich, M., 1996. The effects of copper ions on glutamate receptors in cultured rat cortical neurons. *Brain research*, 742(1-2), pp.211–8.

Weissman, I.L., 2000. Translating Stem and Progenitor Cell Biology to the Clinic: Barriers and Opportunities. *Science*, 287(5457), pp.1442–1446.

Yamada, M. et al., 2007. Electrical stimulation modulates fate determination of differentiating embryonic stem cells. *Stem cells (Dayton, Ohio)*, 25(3), pp.562–70.

Yang, C. et al., 2014. The Potential of Dental Stem Cells Differentiating into Neurogenic Cell Lineage after Cultivation in Different Modes In Vitro. *Cellular reprogramming*, 16(5), pp.1–13.

Zhao, M. et al., 2004. Electrical stimulation directly induces pre-angiogenic responses in vascular endothelial cells by signaling through VEGF receptors. *Journal of cell science*, 117(Pt 3), pp.397–405.

Zhao, M. et al., 2002. Membrane lipids, EGF receptors, and intracellular signals colocalize and are polarized in epithelial cells moving directionally in a physiological electric field. *FASEB journal*, 16(8), pp.857–9.

Tampereen teknillinen yliopisto
PL 527
33101 Tampere

Tampere University of Technology
P.O.B. 527
FI-33101 Tampere, Finland

ISBN 978-952-15-3918-3
ISSN 1459-2045